THESIS APPROVAL

GRADUATE SCHOOL, KASETSART UNIVERSITY

Master of Engineering (Chemical Engineering)
DEGREE

Chemical Engineering	Chemical Engineering
FIELD	**DEPARTMENT**

TITLE: Effect of Cobalt Supported Mixed Phase Mesoporous Silica on Fisher-Tropsch Synthesis Products

NAME: Mr. Prasong Nakaew

THIS THESIS HAS BEEN ACCEPTED BY

_____ **THESIS ADVISOR**

(Associate Professor Metta Chareonpanich, D.Eng.)

_____ **THESIS CO-ADVISOR**

(Associate Professor Paisan Kongkachuichay, Ph.D.)

_____ **DEPARTMENT HEAD**

(Associate Professor Phungphai Phanawadee, D.Sci.)

APPROVED BY THE GRADUATE SCHOOL ON _____

_____ **DEAN**

(Associate Professor Gunjana Theeragool, D.Agr.)

THESIS

EFFECT OF COBALT SUPPORTED MIXED PHASE MESOPOROUS SILICA ON FISHER-TROPSCH SYNTHESIS PRODUCTS

PRASONG NAKAEW

A Thesis Submitted in Partial Fulfillment of
the Requirements for the Degree of
Master of Engineering (Chemical Engineering)
Graduate School, Kasetsart University
2010

Prasong Nakaew 2010: Effect of Cobalt Supported Mixed Phase Mesoporous Silica on Fisher-Tropsch Synthesis Products. Master of Engineering (Chemical Engineering), Major Field: Chemical Engineering, Department of Chemical Engineering. Thesis Advisor: Associate Professor Metta Chareonpanich, D.Eng. 104 pages.

Bimodal porous materials with different pore sizes exhibit several potential applications including catalysis, adsorption, and selective separation due to the fact that their small pores can interact with reactant molecules whereas large pores provide high-speed pathways for the transport of gas and liquid molecules. In this work, the mixed-phase bimodal mesoporous silicas (BMS) were synthesized via sol-gel technique using rice husk ash as the silica source under strong acidic condition, and Pluronic P123 and cetyltrimethyl ammonium bromide (CTAB) as the dual pore structure-directing agent. The molar ratio of SiO_2: Pluronic P123: CTAB: H_2O: HCl of 1: 0.088: 0.088: 4: 2 was used. It was found that the phase separation among SBA-15, SBA-3-like porous silica and xerogel was found when the gel solutions of SBA-15 and SBA-3-like were prepared separately in the primary stage, whereas the mixed-phase uniformly infiltrated SBA-3-like in SBA-15 bimodal porous silica was successfully synthesized when CTAB was added into the SBA-15 gel solution and the secondary micelle structure was formed inside the primary SBA-15 framework. When CTAB and P123 were mixed together in the primary stage, large cluster of aggregation of pseudo-spherical mesoporous primary nanoparticles were synthesized. The obtained bimodal porous silicas were used as the cobalt catalyst supports and tested for the performance of Fischer-Tropsch synthesis reaction. The results were compared to those of monomodal porous silica supports. It was found that the cobalt supported bimodal porous silica presented the higher CO conversion, especially with Co/BMS-1. These catalysts with mixed-phase morphologies significantly promoted the selectivity towards long chain hydrocarbons (C_{5+}). The undesired methane product occurred over monomodal cobalt catalyst was significantly reduced, resulting in the two sizes of cobalt particle occurred in different pore diameters of the bimodal porous silica catalysts.

_____ _____ ___ / ___ / ___

Student's signature Thesis Advisor's signature

ACKNOWLEDGEMENTS

I would like to take this opportunity to acknowledge the people who have helped to make this work possible. My sincere gratitude first goes to my thesis advisor Associate Professor Metta Chareonpanich, for her consistent and thoughtful advice, continuous encouragement and help during the course of this work. Moreover, I am grateful to my graduate committees, Associate Professor Dr. Paisan Kongkachuichay for their kindly giving the time to advice, revise and approve my thesis.

I am grateful to my fellow graduate students at Department of Chemical Engineering, Kasetsart University for assisting me my research and offering valuable suggestion.

The financial supports by the Center of Nanotechnology Kasetsart University and the Graduate School at Kasetsart University, Kasetsart University Research and Development Institute (KURDI) and the National Excellence Center for Petroleum, Petrochemicals and Advanced Materials are acknowledged.

Finally, I would like to thank my family for their love, support, encouragement, and their understanding during the whole period of my education. My family has been my greatest source of strength and inspiration. My gratefulness devotes to my family who wholeheartedly support me aways.

Prasong Nakaew

May 2010

TABLE OF CONTENTS

Page

LIST OF TABLES

LIST OF FIGURES

LIST OF FIGURES (Continued)

LIST OF FIGURES (Continued)

Figure **Page**

Appendix Figure

EFFECT OF COBALT SUPPORTED MIXED PHASE MESOPOROUS SILICA ON FISHER-TROPSCH SYNTHESIS PRODUCTS

INTRODUCTION

A variety of highly ordered mesoporous silica materials, i.e., MCM-41 (Chen *et al*., 1993, Cai *et al*., 2001 and Siriluk and Yuttapong, 2005), SBA-15 (Kruk *et al*., 2000, Escax *et al*., 2007 and Chareonpanich *et al*., 2007), MSU (Bagshaw *et al*., 1995), FDU (Fan *et al*., 2003, 2005), HMS (Tanev *et al*., 1994), and KIT (Kleitz *et al*., 2003), have been successfully synthesized using different synthesis conditions and types of pore structure-directing agents. Such materials have numerous potential applications as adsorbents, molecular sieves and catalyst supports. In all cases, the surface area and pore size of these materials are of essential importance due to the fact that small pores can promote an interaction between porous materials and guest molecules, whereas large pores provide high-speed pathways for guest molecules and the products (Takahashi *et al*., 2007). Therefore, the bimodal porous materials with well-controllable pore sizes and structures are of great interest for catalytic application.

The synthesis of bimodal mesoporous silicas have been investigated by many researchers. The hierarchically structured porous materials for catalysis application could be controlled by using pore texture of different length scales (Coppen *et al*., 2001). The synthesis process of bimodal structure was independently controlled in order to prepare the porous materials with small meso- and large meso- to macroporosity in their framework structure. This method greatly depends on the shape and size of micelles. Chareonpanich *et al.,* (2009) successfully synthesized mixed-phase bimodal mesoporous silicas (BMS) via sol-gel technique from rice husk ash under strong acidic condition using Pluronic P123 and cetyltrimethyl ammonium bromide (CTAB) as the pore structure-directing agent. The molar ratio of SiO_2: Pluronic P123: CTAB: H_2O: HCl of 1: 0.088: 0.088: 4: 2 was used. They found that

the phase separation among SBA-15, SBA-3-like porous silica and xerogel was found when the gel solutions of SBA-15 and SBA-3-like were prepared separately in the primary stage, whereas the mixed-phase uniformly infiltrated SBA-3-like in SBA-15 bimodal porous silica was successfully synthesized when CTAB was added into the SBA-15 gel solution and the secondary micelle structure was formed inside the primary SBA-15 framework. When CTAB and P123 were mixed together in the primary stage, large cluster of aggregation of pseudo-spherical mesoporous primary nanoparticles were obtained.

Nowadays, the interest in solving fossil energy depletion and global warming situation has been intensively grown up. Due to the fuel oil crisis, many researchers have interested to finding the new routes to produce alternative energy for supporting the enormous fuel consumption activities. Furthermore, the trend towards the restriction of the emitted pollutants has been more serious so that high quality of transportation fuels is also needed.

Fischer-Tropsch synthesis (FTS) is a well known catalytic process that very clean alternative fuels can be produced from the conversion of synthesis gas (a mixture of carbon monoxide and hydrogen). Products produced from FTS reaction primarily consist of linear paraffins with low aromaticity and zero sulfur content which are friendly to environment (Van der Laan *et al.,* 1999). Therefore, FTS process is one of the promising solution to produce petroleum-substituted renewable transportation fuels (Knottenbelt, 2002). The synthesis gas used as a reactant substances in FTS reaction can also be produced from carbon dioxide reforming of methane catalytic reaction, so called dry reforming (Kodama *et al.,* 2001). In this process, CO_2 and CH_4 which are greenhouse gases are converted into syngas in the presence of catalyst.

According to the fact that Fischer Tropsch synthesis reactions can be controlled by a number of factors such as support property, metal precursor characteristic, calcination temperature, and so on. Among them, the pore size of the support has a great effect not only on the catalytic activity but also the product

selectivity. For example, the catalytic activity is proportional to the amount of active sites on the surface of catalysts. The increase of active sites can be obtained by dispersing the active metal on the catalyst support. The larger surface area of catalyst supports can provide higher active surface. However, the support with the large surface area usually contains small pore, resulting in poor intra-particle diffusion of both reactants and products which cause the higher CH_4 selectivity and coke deposition. When the support with large pore size is used, the aggregate and low dispersion of metal are often obtained. To overcome this limitation, the bimodal-structure support which contains both large pores and small pores is of great interest since its small pores could provide higher metal dispersion of supported metal crystalline. Furthermore, it is able to diminish the diffusion resistance by the large pores.

In this research, the bimodal mesoporous silicas were synthesized using rice husk ash as a silica source, and Pluronic P123 and cethyltrimethyl ammonium bromide (CTAB) as the dual pore structure-directing agents using the method described by Chareonpanich *et al*., (2009). The bimodal mesoporous silica products were characterized by using N_2-sorption measurements and Transmission Electron Microscopy (TEM). These properties were compared to those of the monomodal mesoporous silica SBA-15 and SBA-3. The obtained bimodal porous silica products were then used as the catalyst support; in this case cobalt metal of specific amount was loaded onto the bimodal porous silica by using wet-impregnation technique. After that, the Fischer-Tropsch synthesis reactions were performed in order to clarify the effect of the bimodal pore structure and the result was compared to those obtained from the monomodal pore structures.

OBJECTIVES

1. To study the effect of bimodal porous silicas on the physicochemical properties of cobalt-loaded bimodal porous silica catalysts.

2. To investigate the role of bimodal porous silica supports on Fischer-Tropsch synthesis performances.

Benefits

1. The influence of bimodal porous silica support on the physicochemical properties of cobalt-loaded bimodal porous silica catalysts is clarified.

2. High selectivity of long chain hydrocarbon products in the range of gasoline to diesel can be achieved over the catalysts prepared by using bimodal porous silica as the support in Fischer-Tropsch synthesis.

LITERATURE REVIEW

Ficher-Tropsch synthesis (FTS) is one of the major routes for converting coal-based and/or natural gas-derived syngas into high quality chemicals and fuels. The main goal of FTS research is to develop FTS catalysts with high activity and selectivity by improving the selectivity of C_{5+} hydrocarbons while decreasing the selectivity of methane. In particular, liquid fuels in the range of diesel fuels produced by FTS (synthesis of hydrocarbons from CO and H_2) exhibit an attractive potential as the very clean alternative energy, relative to the conventional fossil petroleum. The products generated from FTS are mainly composed of linear paraffins with high cetane number and are free of sulfur and aromatic pollutants (Van der Laan and Beenacker, 1999). In order to improve the performances of FTS catalysts and increase the selectivity of the desired hydrocarbon products (C_{10}-C_{20}), informative research understanding is reviewed as the following description.

Fischer-Tropsch Synthesis

In the last decades, the interest in Fischer-Tropsch synthesis has been increased as a result of change in fossil energy reserves, environmental demands and technological developments FTS synfuels have become a key alternative fuel regardless of CO_2 policy because of their low transportation cost and compatibility with existing petroleum infrastructure and vehicles (Takeshita and Yamaji, 2008). In addition, FTS fuels are virtually interchangeable with conventional diesel fuels and can be blended with diesel at any ratio without or with little modification. Concerning carbon monoxide and particulate matter, FTS fuels offer important emission benefits compared with diesel.

1. The Fischer-Tropsch Process

Fischer-Tropsch process is a method for the synthesis of hydrocarbons and other aliphatic compounds principally for producing synthetic petroleum substitutes.

FT process was discovered by Franz Fischer and Hans Tropsch, the German coal researchers, in 1923. This process was invented in petroleum-poor but coal-rich Germany to produce alternative fuels during the World War II. The original Fischer-Tropsch synthesis was described by the following chemical equations:

$$CH_4 + 1/2O_2 \longrightarrow 2H_2 + CO \qquad (1)$$

$$(2n+1)H_2 + nCO \longrightarrow C_nH_{2n+2} + nH_2O \qquad (2)$$

FTS reaction is regarded as a surface catalyzed polymerization process and a lot of heat is involved during reaction. The adsorbed CH_x monomers, formed by hydrogenation of adsorbed CO, react with the surface H atoms and hydrocarbon fragments to produce hydrocarbons with a broad range of chain lengths due to the limitation of the typical Anderson-Schultz-Flory (ASF) distribution (Iglesia, 1997). In this process, synthesis gas can be converted to large ranges of petroleum products such as methane, synthetic gasoline, waxes, alcohols, and water over heterogeneous catalysts (Van Der Laan and Beenackers., 1999; Davis, 2001; Saib *et al.*, 2002). The mechanism of FTS reaction is quite complex because there are many reactions occurred during the reaction (as shown in Table 1) (Iglesia, 1997; Davis, 2001).

2. Mechanism of the Fischer-Tropsch Synthesis Reaction

Although the mechanism of the Fischer-Tropsch synthesis has been studied for more than 70 years, there still was a controversy over the reaction pathway. A mechanism for Fischer-Tropsch synthesis was quite complex and difficult to propose the existent procedures. Unlike many reactions, Fischer-Tropsch synthesis converts two of the simplest compounds, H_2 and CO, into a complex array of products, consisting predominantly of alkenes and alkanes but also varieties of minor compounds including the range of oxygenate compounds. The major mechanisms and modified forms were reported as follows.

Table 1 Major overall reactions in the Fischer-Tropsch synthesis

Main reactions	Chemical equations
1) Paraffins	$(2n + 1)H_2 + nCO \rightarrow C_nH2_{n+2} + nH_2O$
2) Olefins	$2nH_2 + nCO \rightarrow C_nH_{2n} + nH_2O$
3) Water gas shift reaction	$CO + H_2O \leftrightarrow CO_2 + H_2$
Side reactions	
4) Alcohols	$2nH_2 + nCO \rightarrow C_nH_{2n+2}O + (n - 1)H_2O$
5) Boudouard reaction	$2CO \rightarrow C + CO_2$
6) Catalyst oxidation/reduction	$M_xO_y + yH_2 \leftrightarrow yH_2O + xM$
	$M_xO_y + yCO \leftrightarrow yCO_2 + xM$
7) Bulk carbide formation	$yC + xM \leftrightarrow M_xC_y$
Overall reactions	$nCO + (n + 0.5m)H_2 \rightarrow C_nH_m + nH_2O$
	$CO + 2H_2 \rightarrow -CH_2- + H_2O$ ($\Delta H° = -165$ kJ/mol)

Source: Dalai and Davis. (2008)

In the 1950s, the oxygenate (enol) mechanism was achieved widely acceptance. This mechanism involved the chemisorption of CO which reacted with adsorbed hydrogen to form a unit species (as show in Figure 1).

Figure 1 Scheme of the unit species mechanism.
Source: Schulz (1999)

A combination of condensation and water elimination steps by using adjacent groups on the site of active metal resulted in structural growth (Davis, 2001). The enol groups were condensed as depicted in Figure 2.

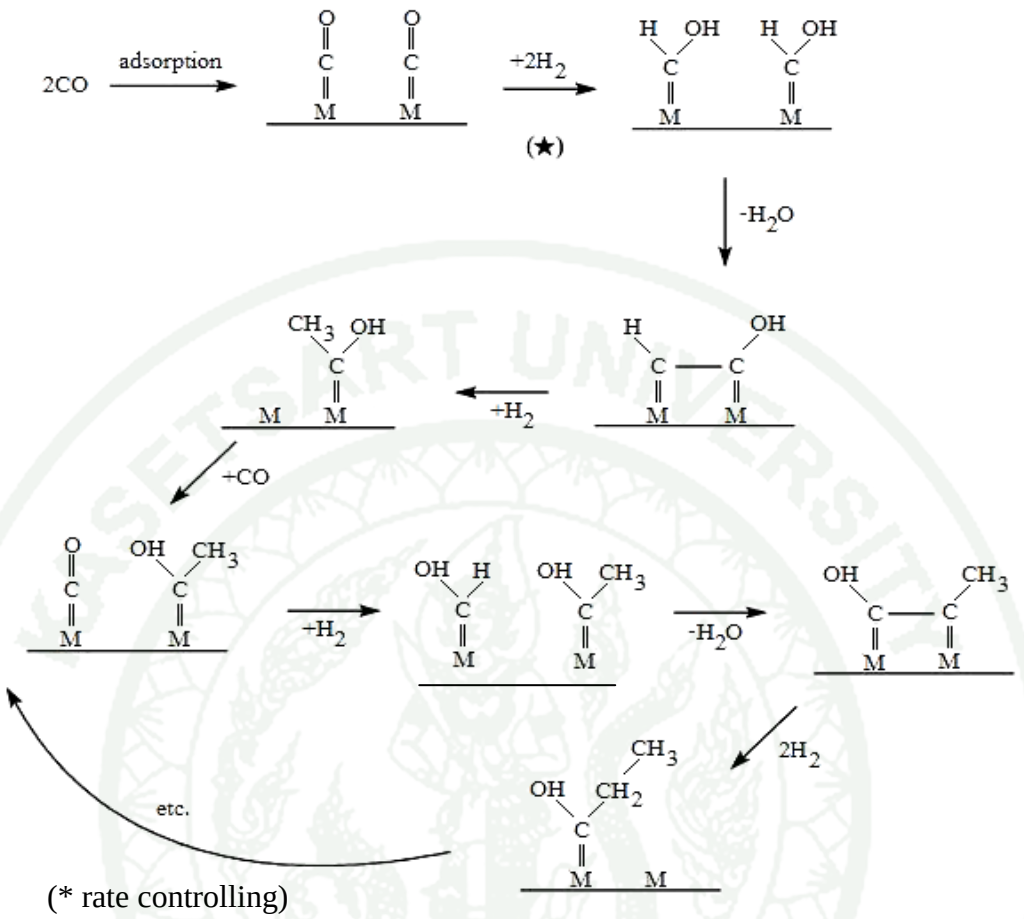

Figure 2 Scheme of the oxygenate (enol) mechanism.
Source: Dry (1996)

Furthermore, the oxygenate mechanism that involved the reaction between CO and adsorbed hydrogen was proposed. The scheme of this mechanism was shown in Figure 3. Besides, an insertion mechanism composed of the insertion of CO into a metal-methyl or metal-methylene carbon bond was also proposed. The inserted metal-methyl or metal-methylene was then hydrogenated to produce an alcohol or alkene; oxygen in the alcohol or alcohol precursor can also be eliminated to produce an alkene product.

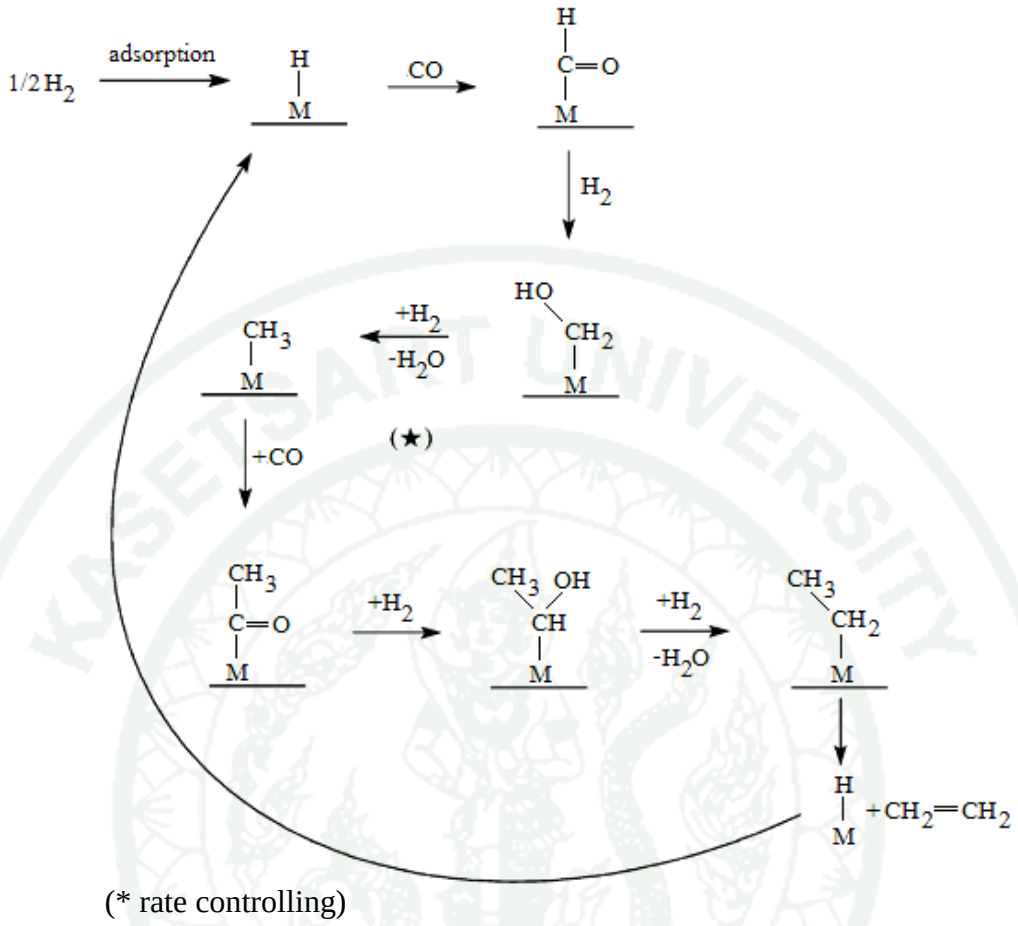

Figure 3 The insertion of CO into a metal-methyl or metal-methylene carbon bond.
Source: Davis (2001)

Davis (2001) also reported the original carbide mechanism for the formation of hydrocarbon and oxygenate products in Fischer-Trpsch synthesis (FTS). The carbide mechanism included the formation of metal carbide followed by the hydrogenation of metal carbide to produce various hydrocarbon products.

With the general availability of surface science instruments, it was found that CO adsorbed on active metal surfaces could produce the surface covered with carbon, and some of oxygen. This phenomenon led to the conclusion that CO was chemisorbed and dissociated to form adsorbed C and adsorbed O. This step was followed by the rapid hydrogenation of adsorbed O to produce water. The

hydrogenation of adsorbed carbon to form CH_2 was much slower. This mechanism was proposed by Maitlis (1989) as shown in Figure 4.

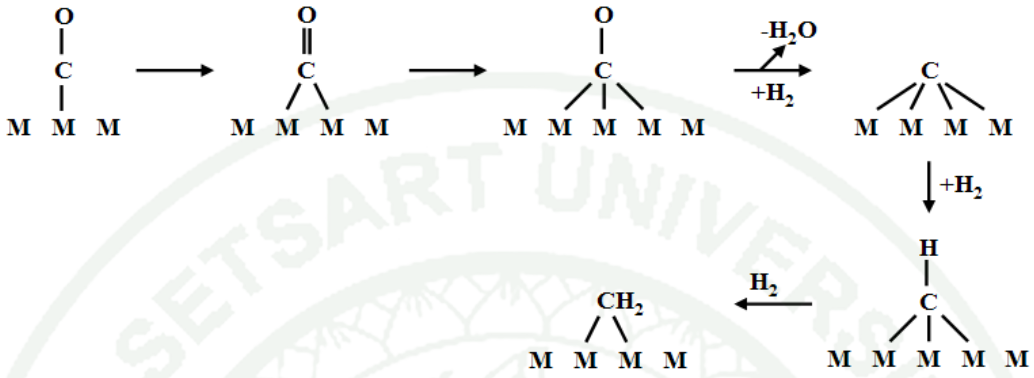

Figure 4 A mechanism for the insertion of CO into a metal-methyl or metal methylene carbon bond.

Source: Davis (2001)

Fischer-Tropsch synthesis had been typically characterized as a surface polymerization since the monomer units were produced from the syngas (hydrogen and carbon monoxide) on the surface of catalyst. In 1999, Steen and Schulz reported the developed equations describing the rate of CO consumption in FTS. As the FTS reaction yielded aliphatic organic compounds and the by-products water and/or carbon dioxide, carbon monoxide was consumed for the formation of organic compounds or carbon dioxide. Therefore, the rate of CO consumption equaled the rate of organic compound formation on carbon basis and could be written as:

$$-r_{CO} = r_{C,\,org} + r_{CO_2} \qquad (3)$$

where $r_{C,\,org}$ is the rate of consumption of CO for the formation of organic compounds in FTS reaction.

According to the polymerization reaction, the formation of organic compounds in FTS was classified featured as three consecutive including initiation, propagation,

and termination (Schulz, 1999). The initiation step could be defined as the formation of a chain starter from CO and H_2. The propagation step was the incorporation of monomer units into growing chain (the chain growth step); the monomer was produced in situ on the catalyst surface during FTS reaction. Finally the termination step was the desorption of growing chains from the catalyst surface. Such that the rate of carbon monoxide for the formation of organic compounds thus equaled the sum of the rate of carbon monoxide consumption in the initiation, propagation and termination steps.

Schultz (1999) also developed the polymerization kinetics of Fischer-Tropsch CO hydrogenation based on an assumption that the rate of reaction in the FTS was controlled by the rate of hydrogenation of surface carbon which was formed through CO dissociation. Surface carbon was hydrogenated and CH_x-surface species was obtained, this reaction was regarded as a chain starter. Figure 5 presents a simplified scheme for the formation of chain starters and incorporation into growing alkyl chains using the polymerization principle.

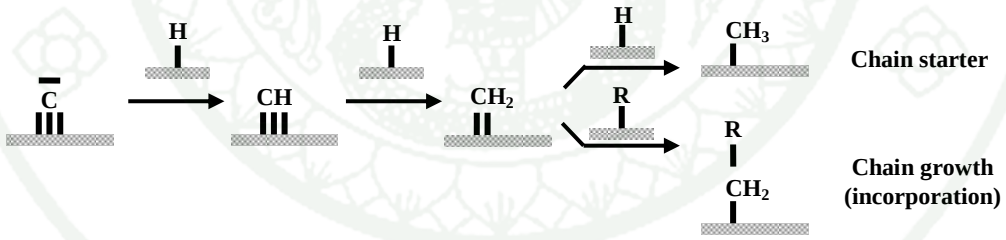

Figure 5 Simplified kinetic scheme of the successive hydrogenation of surface carbon yielding chain starters and incorporation into growing chains.

Source: Schulz (1999)

Moreover, Iglesia (1997) proposed that the FTS reaction produced olefins and paraffins of different chain lengths. This process was basically a chain-building mechanism, where the chain either gained length by adsorbing another CO group, or terminated and left the catalyst as either paraffin or olefin. This was graphically shown in Figure 6.

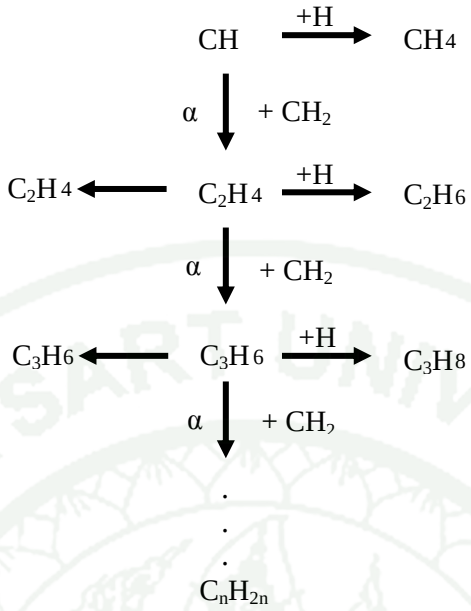

Where α is a chain growth probability

Figure 6 Two possibilities of termination; to a paraffin (right side) or a olefin (arrow to the left), or to grow further with the absorption of CO and H_2 as CH_2.

Source: Iglesia (1997)

As mention above, many researchers proposed the CH_2 insertion as the dominant mechanism for the FTS reaction. However, the formation of oxygenate compounds were hardly possible via the CH_2 insertion mechanism so that oxygenate compounds were assumed to be formed via the CO insertion mechanism. In order to explain both of the formation of hydrocarbons and oxygenates, the formation of CH_2 monomers was proposed and carbide mechanism involving C-O bond dissociation was firstly introduced to react with H_2 to form methylene (CH_2). In 2008, Gaube and Klein proposed a new mechanism of the FTS reaction on iron and cobalt catalysts based on the hypothesis that two incompatible mechanisms were involved on CH_2 insertion and on CO insertion, respectively. The development of the novel mechanism was based on experimental studies of many researchers who employed various types of iron and cobalt catalysts.

3. Fischer-Tropsch Synthesis Catalysts

Fischer-Tropsch synthesis process was shown to be catalyzed by certain transition metals, with cobalt (Co), iron (Fe) and ruthenium (Ru) presenting the noticeably high activity (Vannice, 1977). Cobalt and iron based catalysts were typically applied to FTS process. Moreover, ruthenium and nickel based catalysts also had good activity for FTS, however the availability of ruthenium was limited, thus it was not economically possible. The nickel based catalyst had high activity but methane selectivity was very high, and moreover the performance at high pressure was poor due to the production of volatile carbonyls. Consequently, the FTS reaction was catalyzed focusing on cobalt (Iglesia, 1997 and schultz, 1999) and iron (Luo and Davis, 2003 and Zhang *et al.,* 2006) as practical catalysts.

Nevertheless, the supported Co-based catalysts have been widely used for the synthesis of long chain paraffins (Dry, 1990; Chanenchuk *et al.,* 1991; Iglesia,1997) according to their high activity for syngas conversion and high yields of linear hydrocarbons in FTS reaction at medium reaction temperature and pressure (Iglesia, 1997; Ernst *et al,* 1999). Moreover, Co-based catalysts were more stable toward deactivation by water (by-product of the FTS reaction), less active for the competitive water-gas-shift (WGS) reaction and produced less oxygenates than the Fe-based systems. In order to achieve high amount of surface-active sites (Co^0), cobalt precursors were dispersed on porous carriers such as SiO_2, Al_3O_4 and TiO_2.

3.1 Type of supported catalysts

Due to the fact that different kinds of supports revealed different influences on structure, dispersion and reducibility of cobalt particles (Iglesia *et al*., 1992; Jacobs *et al*., 2002). The advantage and disadvantage of various supports are summarized in detail as follows.

3.1.1 Silica-supported catalysts

Since the interaction between support and cobalt was relatively weak in silica-supported catalysts (Iglesia *et al*., 1992) and this usually leaded to better cobalt reducibility. However, cobalt dispersion was much lower in silica-supported catalysts than in alumina-supported catalysts because the strong interaction of cobalt species with the alumina-supported (Tavasoli *et al*., 2007). Thus, increasing the cobalt dispersion was the major challenge in the design of silica-based Fischer-Tropsch synthesis catalysts. Ernst *et al*., (1999) studied the Fischer-Tropsch synthesis activity and selectivity of Co/SiO_2 prepared by the sol-gel technique in acidic and basic media. They found that the activity in FTS was increased with increasing the specific surface area, and the selectivity for higher molecular weight hydrocarbons was favored in the case of the catalyst with support pore diameter of less than 4 nm. Song and Li (2006) reported the results of cobalt catalysts supported on porous silica with different pore sizes. They found that the large cobalt particles could provide large flat metallic surface, favoring bridge-type adsorbed CO and induced the formation of long chain hydrocarbons. In contrast, small cobalt particles could provide more edges and corners, favoring the CO adsorption in linear geometry of which led to the methane selectivity

3.1.2 Alumina-supported catalysts

Alumina was one of the frequently used supports for cobalt FTS catalysts. However, a major problem due to the use of alumina support was that the cobalt reducibility because cobalt oxide strongly interacted with this support and formed relatively small cobalt crystallites. Chemical reaction of small cobalt particles with the support might result in the formation of cobalt aluminate spinels which decreased the activity and product selectivity in FTS reaction (Chin and Hercules, 1982).

3.1.3 Carbon-supported catalysts

A drawback of oxide support (silica or alumina) was their reactivities towards cobalt, which could lead to form mixed oxides (silicate or aluminate). These mixed oxides were not active in FTS and were reducible only at high temperature. In order to avoid these problems, the use of carbon as a support was explored. Tavasoli *et al.*, (2008) prepared carbon nanofibers as catalyst supports. They found that the strong metal-support interactions were reduced to a large extent and the reducibility of the catalysts was significantly improved. However, the carbon supports caused a slight decrease in the FTS product distribution to lower molecular weight hydrocarbons.

Preparation of Metal Supported Mesoporous Silica Catalysts

Mesoporous silica with unique structural properties had demonstrated a considerable potential for the development of processes and materials designed to meet a range of environmental and technological challenges. The discovery of ordered mesoporous materials with well-defined pore sizes within the range of 2-50 nm, regular channel systems, high thermal stability and the potential for the isomorphous substitution could promote new opportunities in material chemistry and catalysis (Kresge *et al.*, 1992; Beck *et al.*, 1992; Inagaki *et al.*, 1993; Zhao *et al.*, 1998).

1. Monomodal mesoporous silica support

Periodic mesoporous silicas have attracted great attention to many researchers to use as catalyst support materials. Narrow pore-size distribution, high surface area and pore volume make them suitable as the excellent supports for metal and metal oxide catalysts (Zhao *et al.*, 1998; Zholobenko *et al.*, 2001). Two most common types of periodic mesoporous silica are MCM-41 and SBA-15. MCM-41 materials were usually synthesized in basic mediums, while SBA-15 materials were typically prepared in acidic conditions. SBA-15 materials had larger pore than MCM-41 and

the pore size could be adjusted from 2 to 30 nm at the stage of synthesis by using various surfactants and different reaction conditions (Coma, 1997; Zhao *et al.*, 1998; Zholobenlo *et al.*, 2001). In addition, SBA-15 material with high specific surface area and pore wall thickness, 2D hexagonal pore-arrangement, and controllable uniform mesopore diameters had attracted great attention for large number of applications in catalysis and separation (Guari *et al.,* 2001; Konya *et al.,* 2002; Mirji *et al.,* 2007). Recently, SBA-15 material was commercially used as a catalyst support and represented good properties for catalytic reaction according to their large internal surface area (~1,000 m^2/g) and narrow pore size distribution.

During the last several years, SBA-15, which is the polymer-templated silica with hexagonally ordered mesopores, has been extensively studied and evaluated for numerous applications in the field of catalysis and separations (Zhao *et al.,* 1998; Selvaraj *et al.,* 2002; Jana *et al.,* 2003; Tuel *et al.,* 2004; Grieken *et al.,* 2006). In 2004, Ohtsuka *et al*. prepared mesoporous molecular sieves (MCM-41 and SBA-15) with different pore diameters and used as high loading supports of cobalt catalysts. The performances of the cobalt catalysts in FT synthesis were comparatively studied. Template ion exchange method and conventional impregnation method were used to incorporate cobalt into the support framework. SBA-15 mesoporous silica with larger pore diameter compared to MCM-41 material exhibited higher CO conversion in FTS reaction. The catalyst with pore diameter of 8.2 nm showed the highest CO conversion of 72 %. In addition, Saib *et al.,* (2002) reported that MCM-41 support with smaller pore size compared to that of SBA-15, could lead to the formation of smaller cobalt oxide particles, where were more difficult than the larger particles to reduce to metal because of the stronger interaction between metals and support.

In addition, the thicker pore wall of SBA-15 compared to that of MCM-41 exhibited the different behavior of mesoporous silicas. SBA-15 had higher thermal stability compared to MCM-41, as a result, SBA-15 structure was not destroyed during the preparation process, i.e., drying, calcination and impregnation (Khodakov *et al.,* 2005). Another feature of SBA-15 was the existence of micropores interconnecting hexagonally ordered mesopores, which made it more suitable for

catalysis because the interconnection facilitated diffusion inside the entire porous structure (Shah *et al.*, 2007).

In 2005, Nanta-ngern successfully synthesized SBA-15 mesoporous silica with average pore diameter of 9 nm from rice husk ash under strong acidic condition using Pluronic P123 as the structure-directing agent. The molar ratio of SiO_2 : Pluronic P123 : H_2O : HCl of 1: 0.0875 : 200 : 4 was used. The highly ordered pore structure of SBA-15 (as shown in Figure 7) was obtained at the hydrolysis-condensation temperature of 40 °C for 24 h and hydrothermal aging temperature of 100 °C for 24 h.

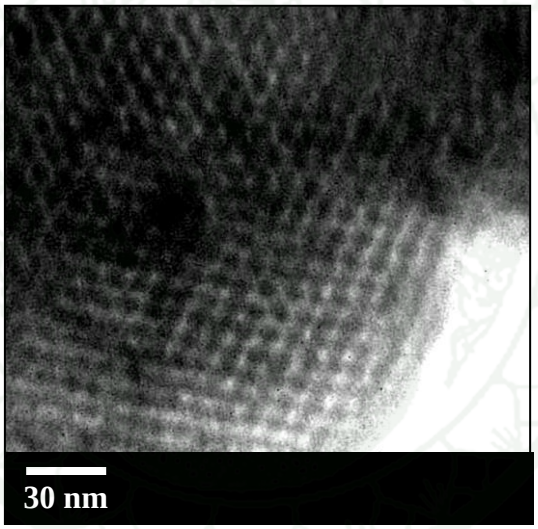

Figure 7 TEM image of SBA-15 synthesized at the molar ratio of 1 SiO_2 : 0.00875 Pluronic P123 : 200 H_2O : 4 HCl.

Source: Nanta-ngern (2005)

2. Bimodal mesoporous silica support

Bimodal porous materials are materials having pores of two different sizes including micro-mesopore, micro-macropore, and meso-macropore. Among these groups of materials, the active surfaces of small pores can interact with molecules, whereas large pores provide high-speed pathways for the transport of gas and liquid

molecules (Takahashi *et al*., 2007). The bimodal porous materials have several applications including catalysis, adsorption, and selective separation, where both molecular transportation and interaction between solid surface and molecules occur simultaneously.

The binary surfactant systems are applied to produce products with tunable pore sizes and bimodal or trimodal pores. By simply blending two quaternary cationic surfactants with different carbon chains together (e.g., C_{12}TAB and C_{16}TAB, C_{16}TAB and C_{22}TAB), the pore sizes of MCM-41 mesostructures were changed to intermediate values between the values templated by a single surfactant. Hierarchical pore structures are also beneficial for special applications. Multimicellar systems and assemblies of nanoparticles with small mesopores possibly promote the foundation bimodal and also trimodal pore architectures. It should be emphasized that the creation of hierarchical micellar systems is usually unfavorable from a general thermodynamic point of view. The mixture of most cationic surfactants, whose products have small mesopores, and block copolymers, which template comparatively large mesopores, always results in either phase separation or compound micelles. The latter favors the formation of uniform large mesopores. However, the properties of surfactants themselves should be thoroughly considered in the mixture, for example, the hydrophobic/hydrophilic balance of the block copolymer by the addition of ionic surfactants, the interactions such as hydrogen bonding and polar interactions between the head groups of ionic surfactant and block copolymer micelles (Wan and Zhao, 2007).

Sun *et al*., (2003) studied to synthesis of bimodal mesoporous silica structured by chemical templating-scaffolding route that enabled independent control over small and large mesopore sizes. Mesoporous MCM-41 was synthesized in a first step and cross-linked a bimodal porous material. Triblock copolymer surfactants added later formed assemblies around which the nanoparticles aggregated and cross-linked, considerably, influencing both the average and the width of the secondary pore size distribution, without affecting the primary pore size. By changing the conditions of

the second step, a broad variety of silicas with a controlled bimodal nanopore size distribution could be easily synthesized.

Shinoda *et al*., (2004) studied the synthesis of bimodal pore support developed by introducing silica (pore size 5 nm) or ZrO_2 sols (pore size 1.7-2.4 nm) into large pores of SiO_2 gel pellets (pore size, 50 nm) directly. The bimodal pore supports were obtained. On the other hand, the increased BET surface area and the decrease of pore volume compared to those of original silica gel indicated that the obtained bimodal pore supports formed according to the designed route. The obtained bimodal pore supports were applied in liquid-phase Fischer–Tropsch synthesis where cobalt was supported and presented the excellent reaction performance with higher reaction rate and lower methane selectivities. They suggest that the spatial effect of bimodal pore structure and chemical effect of the porous zirconia promoted the FTS reaction.

Zhang *et al*., (2004) synthesized of bimodal mesoporous aluminosilicates by using sol–gel method and cetyltrimethylammonium bromide (CTAB) as the structure-directing agent. Ordering-packed framework mesopore was created within the colloidal particles by the templating function of surfactant CTAB and disordered textual pore was formed by the aggregation of colloidal particles as an inter-particle pore. As a result, the hydrothermal stability and catalytic life of the material was highly improved for the catalytic cracking reactions.

In 2009, Chareonpanich *et al.,* successfully synthesized mixed-phase bimodal mesoporous silicas (BMS) via sol-gel technique from rice husk ash under strong acidic condition using Pluronic P123 and cetyltrimethyl ammonium bromide (CTAB) as the pore structure-directing agent. The molar ratio of SiO_2 : Pluronic P123 :CTAB: H_2O : HCl of 1: 0.088 : 0.088 : 4: 2 was used. They found that the phase separation among SBA-15, SBA-3-like porous silica and xerogel was found when the gel solutions of SBA-15 and SBA-3-like were prepared separately in the primary stage, whereas the mixed-phase uniformly infiltrated SBA-3-like in SBA-15 bimodal porous silica was successfully synthesized when CTAB was added into the SBA-15 gel solution and the secondary micelle structure was formed inside the primary SBA-15

framework. When CTAB and P123 were mixed together in the primary stage, large cluster of aggregation of pseudo-spherical mesoporous primary nanoparticles were obtained. The highly ordered pore structure of bimodal mesoporous silicas (as shown in Figure 8) was obtained at the hydrolysis-condensation temperature of 40 °C for 24 h and hydrothermal aging temperature of 100 °C for 24 h.

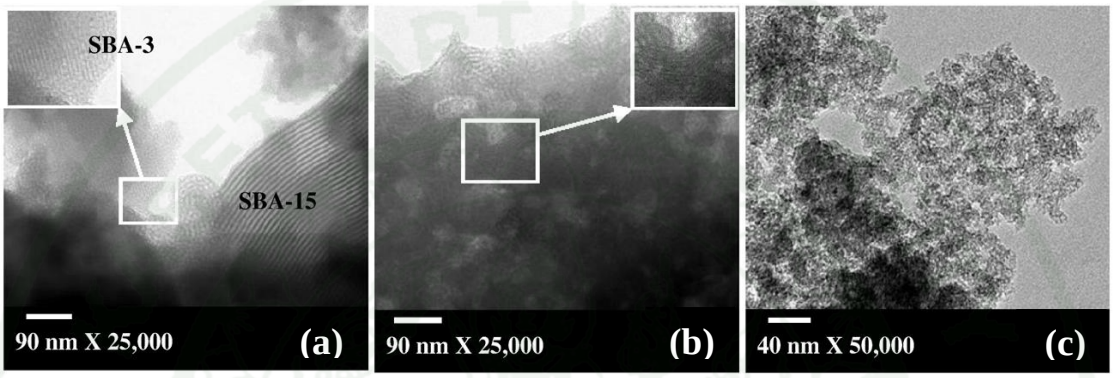

Figure 8 TEM images (a, b, c) of bimodal mesoporous silicas synthesized from various mixing sequences.

Source: Chareonoanich *et al.*, (2009)

Tavasoli *et al*., (2007) reported that the high cobalt dispersion was obtained by the deposition of a cobalt salt on the supports such as silica and alumina. Conventional monomodal support with a large surface area usually contains small pores, resulted in poor intra-pellet diffusion of reactants and products, especially in multiphase reactors. Moreover, slow transportations of reactants and products to and from catalytic sites often control the rate of primary and secondary reactions. In the case of bimodal porous material supports having large pores and small pores, small pores provided the sites for supporting small cobalt particles, while the large pores provided a network for fast diffusion of reacting molecules and products. The typical pore size distribution in bimodal porous silica is shown in Figure 9. The catalytic performance in FTS reaction of cobalt loaded on the bimodal and monomodal porous silica support was reported by Tsubaki *et al.*, (2001). They found that the cobalt loaded on bimodal support gave higher CO conversion and lower CH_4 selectivity compared to that of monomodal supports.

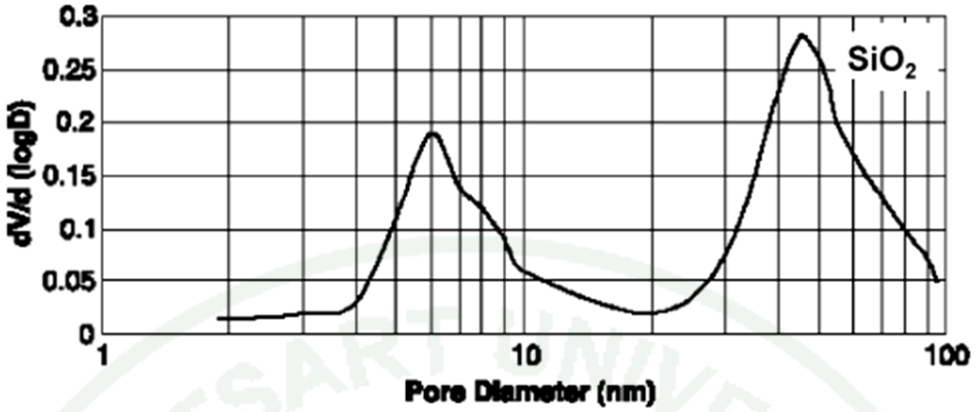

Figure 9 Pore size distribution of bimodal catalyst support.
Source: Tsubaki *et al*. (2001)

2. Effect of Catalyst Preparation on FTS Performances

The selectivity towards the desired products is the main subject in FTS performances. One of the most important product selectivity is the selectivity of C_{5+} hydrocarbon products. Because the ultra clean liquid fuels are of industrial interest, it is essential to improve the performances of FTS by increasing the C_{5+} selectivity and suppress the formation of undesired methane in FTS products. Either the properties of synthesized catalyst support or the methods or chemicals used in catalyst preparation have direct influence on FTS catalytic performance. The regarding information is presented as follows.

2.1 Effect of Catalyst Support on FTS Performance

In fact, it was well-known that the catalytic conversion of carbon monoxide occurred on the surface of porous catalyst. For this reason, the structure of catalyst support greatly affected the orientation of metal particles locating on the surface of catalyst support. Many studies have been carried out on Fischer-Tropsch synthesis using different supports for cobalt loading, including alumina (Bechara *et*

al., 2001 and Hosseini *et al.*, 2004), titania (Zennaro *et al.*, 2000) and silica (Khodakov *et al.*, 1997; Sun *et al.*, 2000; Tsubaki *et al.*, 2001).

In 2002, the study of the influence of average pore diameter of silica support on the physical and chemical properties of supported cobalt catalysts and their performances in FT synthesis were carried out by Saib *et al.*, The metal crystallite size and degree of reduction were higher with increasing pore diameter of the support from 4 nm or larger. For the impregnated catalysts, the metal crystallites seemed to appear in clusters on the surface of catalyst support and when the average pore diameter increased, the size of cobalt clusters also increased.

Li *et al*. (2006) investigated the influence of pore size on the distribution of cobalt species and catalytic properties of Co/MCM-48, Co/SBA-15 and Co/SiO_2 on FTS reaction. The catalysts with 15 wt.% Co loading were prepared by incipient wetness impregnation method. As a result, the Co_3O_4 crystallites sizes were controlled by the support pore diameter in mesoporous silicas. The order of decreasing average Co_3O_4 crystallite diameter was Co/SBA-15 > Co/SiO_2 > Co/MCM-48, and the C5+ selectivity of the catalyst was also followed this sequence. The low reducibility of the large amount of small cobalt particles and cobalt silicates formed on Co/MCM-48 led to lowest activity and C5+ selectivity. The low dispersion for Co/SBA-15 led to loss of active cobalt metal sites.

SBA-15 mesoporous silicas were concerned as a good catalyst support to synthesize long chain hydrocarbons according to their large pore diameters. Khodakov *et al.*, (2002) determined the pore size effects on the FTS reaction rate and selectivity over cobalt catalysts using SBA-15 and MCM-41 mesoporous silicas as catalytic supports. As a result, the cobalt catalysts with pore diameter exceeded 3 nm provided much higher reaction rate and C_{5+} selectivities. Furthermore, the size of cobalt particles and the degree of reducibility in wide pores (SBA-15) and narrow pore (MCM-41) were different. The larger pore diameter led to the larger size of supported cobalt species. The supported catalyst with pore diameter of 10 nm was found to be the most active and selective catalyst for hydrocarbon formation in FTS reaction (Khodakov *et al.*, 2003). Similarily, Ohtsuka *et al.*, (2004) also reported that

the performance of Co support SBA-15 catalyst in the FTS reaction was higher than that of MCM-41 supported catalyst. The Co/SBA-15 catalyst with the pore diameter of 8.3 nm gave highest conversion (72 %) and efficient production of C_{10}-C_{20} fraction as the main component of diesel fuel.

3.2 Effect of metal loading and dispersion on catalytic performance

The dispersion of metal species on catalyst support have significant role on catalytic FTS performance. Higher concentration of cobalt metal sites favors higher rate of FTS reaction. Therefore, cobalt dispersion and reducibility are concern as the important parameters affecting the number of cobalt surface sites and thus the overall catalytic performance (Iglesia, 1997).

Catalytic activity and selectivity are also strongly influenced by the surface properties of the support because they can change the interaction between cobalt and the support, resulting in different dispersion and reducibility of the supported cobalt. In 2003, Khodakov *et al.*, reported the effect of support structure on the cobalt dispersion. Two types of silicas were used as the catalytic supports including SBA-15 mesoporous silica with pore diameter of 9.1 nm and narrow pore size distribution, and the commercial mesoporous silica (Cab-osil M5) with pore diameter of 33 nm and broad pore size distribution. The results showed that metal dispersion was better when SBA-15 material was applied. This was because SBA-15 led to higher cobalt dispersion and also prevented cobalt particles from sintering.

In addition, metal precursors and pretreatment conditions mainly influenced the structure and catalytic performance of Co/SiO_2. Although the silica support promoted high reducibility according to weak interaction between metal and silica support, they favored the agglomeration of supported cobalt particles. A solid-state reaction of silica and cobalt oxides also resulted in cobalt silicate (mixed oxide) which played negative role on the catalytic performance (Coulter and Sault, 1995).

In 2005, Girardon *et al.*, prepared the FTS catalysts via aqueous impregnation of silica using cobalt nitrate and cobalt acetate as metal precursors. Significantly, they reported that higher dispersion was found with the catalyst prepared from cobalt nitrate, whereas the catalyst prepared from cobalt acetate generated cobalt silicate as a dominant phase which caused more difficult reducibility and larger agglomeration of cobalt clusters. The low cobalt dispersion was attributed to the sintering of Co_3O_4 crystallites at high temperature. From this research work, it can be concluded that types of metal precursors strongly affected the dispersion of cobalt species on silica support.

Interestingly, Reubroycharoen *et al.*, (2006) reported that the drying process also played an important role on the dispersion of active metal sites. The conventional heating method, which drying oven was applied, caused gas flowing inside out from the support. When volatile matters within the catalyst support were not completely removed, the flowing gas resulted in an accumulation of the active species on the outer surface of support, thus low metal dispersion was found. Instead of preparing catalysts by conventional drying and calcination, the commercial microwave oven was applied in drying and calcination process of impregnated catalysts to overcome this undesired phenomenon. It can be seen that the cobalt species prepared by microwave irradiation were more uniform and had better dispersion within catalyst pellets compared to that prepared by the conventional heating method. The rapid drying of microwave irradiation caused uniform particle size and distribution of Co/SiO_2 (as shown in Figure 9) while the conventional method displayed the partly agglomeration of cobalt particles on the surface.

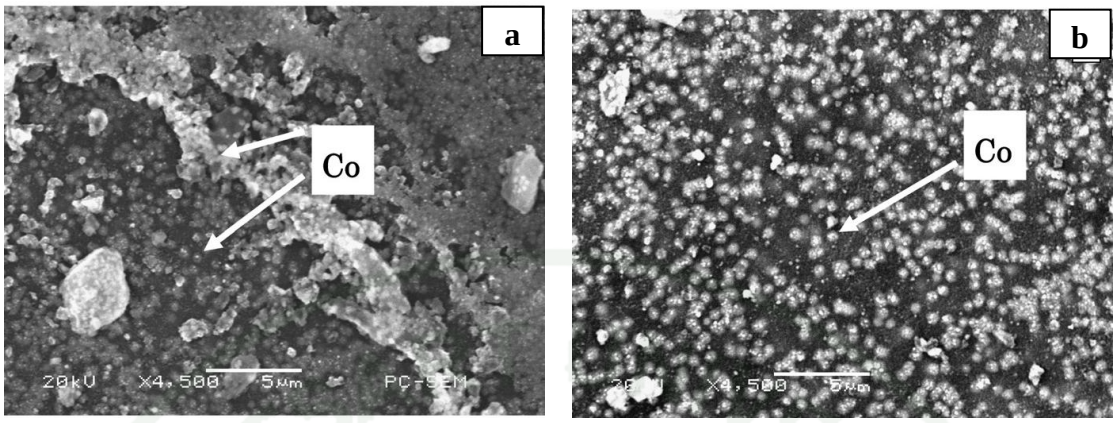

Figure 10 SEM images of Co/SiO_2 catalysts: (a) conventional heating catalyst (b) microwave irradiation catalyst.

Source: Reubroycharoen *et al*., (2007)

It is usually suggested that the size of supported metal and oxide particles and thus their catalytic behavior principally affected by overall metal content in supported catalysts. It is generally assumed that an increase in metal loading would almost automatically result in lowering of metal dispersion. In 2006, *Li et al*., investigated the amount of cobalt loading affected the surface reaction parameter during CO hydrogenation. Co/MCM-48 catalysts were prepared using incipient wetness impregnation method with cobalt loading of 5, 10 and 15 wt.% respectively. They found that for 5 wt.% cobalt loading presented high density of cobalt crystallites on the external surface. The reducibility and FTS catalytic behavior of cobalt species supported by MCM-48 were affected by Co loading. Lower FTS activity and higher methane selectivity observed on 5 wt.% Co loading catalyst were principally attributed to the low reducibility of small cobalt particles. With increasing the loading amount, the cobalt crystallite size increased (as shown in Figure 11) and led to higher reducibility and C_{5+} selectivity. But when Co loading exceed 10 wt.%, the CO conversion and hydrocarbons selectivity seemed to affect slightly by Co loading.

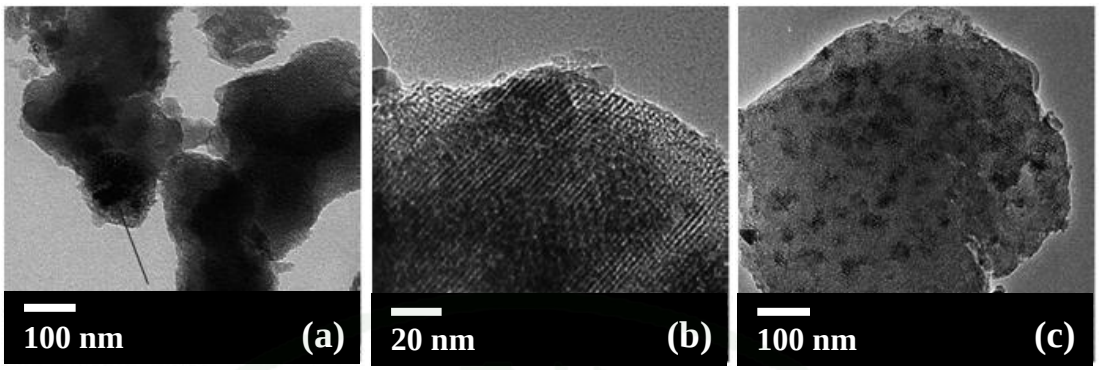

Figure 11 TEM micrographs of (a) 5 wt.% Co/MCM-48, (b) 10 wt.% Co/MCM48 and (c) 15 wt.% Co/MCM-48.

Source: Li *et al*. (2006)

In 2003, Khodakov *et al*. studied the impact of cobalt content on cobalt dispersion and catalytic performance. In this research, two series of cobalt catalysts supported by S1 and S2 silicas with a wide range of cobalt loadings (10–40 wt.%) were prepared. They found that cobalt introduction to silicas led to a decrease both in BET surface area and total pore volume. This effect was especially pronounced for the catalysts with higher cobalt loadings. The decrease in BET surface area and pore volume was likely to be principally due to plugging support pores by cobalt species. Even in catalysts with high cobalt contents, the sizes of supported particles of Co_3O_4 were strongly affected by silica pore diameters. The presence of narrow pores could lead to higher cobalt dispersion. Narrow pore size distribution in periodic mesoporous silicas seems to prevent cobalt particles from sintering. Catalytic behavior of silica supported cobalt catalysts in FT synthesis was found to depend on the nature of cobalt species, cobalt particle size and catalyst mesoporous structure. The maximum CO conversion was obtained for the catalyst loaded with ca. 30 wt.% Co, presenting the highest density of surface Co^0 sites.

The information regarding the CO conversion of different mesoporous catalysts with low amount of cobalt loading are summarized in Table 2.

Table 2 CO conversion of mesoporous catalysts with low cobalt loading

Catalysts	Support	X_{CO} (%)	Condition	Reference
5Co/MCM-48	MCM-48	6.5	H_2/CO=2, SV of syngas 2 S L $g^{-1}h^{-1}$, temperature 270 °C, pressure 10 bar.	*Li et. al., 2006*
10Co/MCM-48	MCM-48	27.1		
5Co/Al_2O_3/nitrate	Al_2O_3	12.1	H_2/CO=2, flow rate 30 ml/min, temperature 250 °C, pressure 1 bar	*Loosdrecht et. al., 1997*
5Co/Al_2O_3/citrate	Al_2O_3	5.2		
5Co/SBA-15	SBA-15	8.2	H_2/CO=2, GHSV of syngas 13.5(NTP)/(gcat h), temperature 220 °C, pressure 20 bar	*Martinez et. al., 2003*
5.7Ti-Co6	Rutile titania	12.5	H_2/CO=1.83, flow rate 20 ml/min temperature 221 °C, pressure 5.5 bar	*Bertole et al., 2004*

From the information reported above , further consideration should be focused on the impact of cluster size on the reducibility of cobalt clusters. At low cobalt loadings, the cobalt oxide–support interaction was strengthened, making it difficult to achieve the complete reduction of the cobalt clusters and therefore, surface active sites were hardly generated.

3. Metal Loading Techniques

Mesoporous silica itself is not a suitable catalyst for FTS reaction since it has less activity. However, due to its unique characteristics, it can be applied as a catalyst support material especially cobalt metal for FTS reaction or a catalytic site by partial substituting Si^{4+} by another cations (Lou *et al*., 2008). Therefore, it is a great

importance to introduce metal atoms with good dispersion into the mesoporous silica framework. A simple way to fuctionalize SBA-15 mesoporous silica is to introduce active metal ions into the silica metrix either during the synthesis (direct synthesis) or by post-synthesis modification . The details of metal loading techniques are described as follows.

3.1 Post Synthesis Method

As far as we know, most of research works reported the metal containing SBA-15 materials prepared by the post-synthesis method. Different strategies of synthesis may lead to major changes in bonding and environment of metal species within SBA-15 mesoporous silica (Li *et al.,* 2005). Generally, impregnation is the most common method for cobalt-containing mesoporous silica synthesis. By using this method, mesoporous catalyst supports are impregnated by various types of cobalt salt solutions, for example cobalt acetate, cobalt nitrate (Bhoware *et al.,* 2006; Mochizuki *et al.,* 2006) and cobalt sulphate (Lou *et al*., 2008).

Co-based catalysts were widely prepared by an impregnation method followed by drying, calcination and H_2 reduction (Reuel and Bartholomew, 1984). Cobalt nitrate, a conventional Co precursor, was considered to decompose to Co_3O_4 species by drying and calcination process (Ernst *et al.,* 1984; Bian *et al.,* 2003). During H_2 reduction, the Co_3O_4 species were reduced to CoO species and then consecutively reduced to metallic Co or Co-SiO_2 interaction species (Ming and Baker, 1995 and Khodakov *et al.,* 1997).

Martinez *et al.,* (2003) prepared mesoporous Co/SBA-15 catalysts for the Fischer-Tropsch synthesis by using impregnation method. The influence of cobalt loading, cobalt precursor, and promoter were investigated. For Co/SBA-15 catalysts prepared from cobalt (II) nitrate, the dispersion of cobalt species was increased and the extent of cobalt reduction was increased with the amount cobalt loading. A maximum CO conversion was found for the catalyst with approximately 30 wt.% Co loading. Moreover, they found that the addition of 1 wt. % Rhenium enhance the

reducibility of cobalt oxides and increased the catalyst activity. Rhenium could promote the formation of long chain hydrocarbons (C_{10+}) while decreasing methane selectivity. Cobalt dispersion was also improved by the promotion of Mn but the degree of reducibility was decreased, producing catalysts with less active than the unpromoted catalyst.

In 2007, Zhang *et al.* prepared silica-supported cobalt (20 wt. %) catalysts by incipient-wetness impregnation. In order to study the effects of impregnation solvent on Co/SiO_2 catalysts, different cobalt nitrate solutions including ethanol and aqueous solutions were used to prepare the cobalt catalysts. They found that the catalyst activity greatly depended on the type of impregnation solvent. The size of cobalt particles prepared from ethanol dehydration was smaller and more uniform than that of the aqueous solution at the same amount of cobalt loading. However, its reducibility was slightly poorer than that of cobalt catalyst impregnated by aqueous solution. The lower reduction degree of cobalt supported catalyst impregnated by ethanol solution could be ascribed to the decrease of polarity of the solvent, which increased the interaction between cobalt complex and silica surface. Using ethanol as impregnation solvent promoted the distribution of Co over the silica surface, resulting in higher dispersion of supported cobalt. Moreover, the catalyst prepared from dehydrated ethanol solution was considered to increase amount of active sites and more reactive adsorbed CO on the surface in liquid-phase FTS reaction, showing high catalyst activity and low methane selectivity.

The cobalt catalysts prepared by the post synthesis method somehow play negative role on catalytic performances. In 2006, Bhoware and Singh, studied the performances of cobalt containing MCM-41 catalysts prepared by three different methods including grafting, direct hydrothermal and immobilization methods. The experimental results showed that the BET surface area of cobalt supported catalysts prepared by grafting and immobilization methods (post-synthesis method) were sharply decreased from 1,010 to 820, and 700 m^2/g, respectively. In contrast, the cobalt catalysts prepared by the direct hydrothermal method, the substitution of cobalt species into silica framework occurred and the specific surface area was slightly

increased from 1,010 m^2/g to 1,050 m^2/g. As a result, cobalt supported catalyst prepared by the direct hydrothermal technique exhibited higher conversion than that of grafted and immobilized catalysts in the catalytic reaction.

3.2 Direct Synthesis Method

Post-synthesis methods have the disadvantage of uncontrolled growth of metal particles on the surface of catalyst support since no preventive measures are taken to ensure the metal precursors isolation within the channels. So, the preparation of metal supported catalysts with high degree of metal dispersion is one of the major challenges in the design of silica-based FTS catalysts. It would be very useful to explore better and simpler methodologies for localizing metal nanoparticles within the mesochannels while retaining high surface area and pore volumes which for catalysis instead of post-synthesis methods, i.e., impregnation and grafting techniques (Prashar *et al.,* 2008).

The alternative way to introduce cobalt species into the mesoporous silica framework is an addition of cobalt precursor into the synthesis mixture, followed by hydrothermal treatment; so called the direct synthesis method (Yang *et al.,* 2007; Lou *et al.,* 2008). The incorporation of transition metals into the framework of SBA-15 silica by direct synthesis had become a very attractive goal for many researchers because the heteroatom incorporation into the silica structure could be carried out in only one step and more stable metal species were obtained (Melero *et al.,* 2005). Furthermore, the preparation of catalysts with well-dispersed isolated metal species was very important in order to obtain high activity and selectivity for the catalytic reactions (Bharat *et al.,* 2001; Wang *et al., 2005*; Selvaraj and Kawi, 2008; Aguado *et al*., 2008). It is still a challenge to find a one-step route of metal incorporation into SBA-15 in order to increase the catalytic performance without changing its structural order or the complexity of the synthesis. For this reason, the direct synthesis method is a crucial way to effectively synthesize highly dispersed metal or metal oxide-containing SBA-15 mesoporous silica.

Many efforts have been devoted to the study of incorporating transition metals into SBA-15 framework for a variety of application. Bharat *et al.,* (2000) attempted to achieve a high degree of Ti substitution without the loss of textural properties, especially pore size of SBA-15. The Ti/SBA-15 catalysts were prepared via the direct synthesis method under microwave-hydrothermal conditions. In addition, Vinu *et al.,* (2005) reported that the main approach used to incorporate iron atoms into SBA-15 silica was a simple adjustment of the pH of gel mixtures above the isoelectric point of silica (pH~2). In this conditions, the negative charge of silica species can easily interact with the positive charge of iron complex, resulting in incorporation of larger quantities of Fe into the SBA-15 mesoporous silica matrix.

As mentioned above, it is clearly seen that the bimodal porous silica is a promising support for cobalt-based Fischer-Tropsch synthesis catalyst. In this research, the novel bimodal mesoporous silica synthesized by using Pluronic P123 and CTAB as the dual pore structure-directing agents similar to the procedure described by Chareonoanich *et al.*, (2009) was used as the cobalt supports. The monomodal porous silica was also used to compare the effect of bimodal mesoporous silica. The physical and chemical properties of catalysts and their catalytic performances were investigated. Moreover, the cobalt phases and the amount of carbon deposition were further investigated in order to clarify the effect of the existence of bimodal pore structure.

MATERIALS AND METHODS

In this chapter, the information including the chemicals and instruments, and the experimental procedures of supports and catalysts preparation including the FTS performance were explained. In the first part, chemicals and devices used in the preparation of catalysts, testing units of FT synthesis performances, and product analysis unit were explained. The methods of catalyst synthesis and catalyst performance testing were then reported in the latter part. The preparation of silica support, metal loading techniques and the investigation of FT synthesis reaction were explained in detail.

Chemicals and Equipments

1. Chemicals

The chemicals used for catalyst preparation and Fischer-Tropsch synthesis reaction are listed below.

1.1 Chemicals for Catalyst Preparation

1.1.1 Rice husk ash used as a silica source was refluxed with 1 L of 1 M HCl solution for 2.5 h, washed with distilled water and dried at 120 ^{o}C (Figure 12).

Figure 12 Photo of rice husk.

1.1.2 Pluronic P123 ($PEO_{20}PPO_{70}PEO_{20}$, Aldrich)

1.1.3 Cobalt nitrate ($Co(NO_3)_2 \cdot 6H_2O$, 99.0% purity, UNIVAR)

1.1.4 Cethyltrimethyl ammonium bromide ($C_{16}H_{33}N(CH_3)_3$-Br, CTAB, AJAX, No. A147)

1.1.5 Sodium hydroxide (NaOH, 99% purity, Merck)

1.1.6 Hydrochloric acid (HCl, 36.5-38.0 wt% purity, J.T. Baker)

1.1.7 Distilled water

1.2 Chemicals for Fischer-Tropsch Synthesis Reaction

1.2.1 Reactant gases

- Carbon monoxide (CO, 99.2% purity, TIG)
- Hydrogen (H_2, 99.99% purity, TIG)
- Nitrogen (N_2, 99.99% purity, TIG)
- Oxygen (O_2, 99.5% purity, Linde)

1.2.2 Standard gases

Mixture of 5% carbon monoxide (CO), 5% carbon dioxide (CO_2), 5% methane (CH_4), 5% ethylene (C_2H_4), 5% ethane (C_2H_6), 5% propylene (C_3H_6), 5% propane (C_3H_8), 5% i-butane (C_4H_{10}), 5% n-butane (C_4H_{10}) in helium (He) balance (SOXAL) was used as the standard gases.

1.2.3 Standard liquid hydrocarbons

- n-Pentane (n-C_5H_{12}, 99.64 % purity, Fischer chemicals)
- n-Hexane (n-C_6H_{14}, 99 % purity, Merck)
- n-Heptane (n-C_7H_{16}, 99.5 % purity, Fluka)
- n-Octane (n-C_8H_{18}, 99 % purity, Merck)
- n-Nonane (n-C_9H_{20}, 99 % purity, Merck)
- n-Decane (n-$C_{10}H_{22}$, 99 % purity, Merck)
- n-Undecane (n-$C_{11}H_{24}$, 97 % purity, Fluka)
- n-Dodecane (n-$C_{12}H_{26}$, 99 % purity, Merck)
- n-Tridecane (n-$C_{13}H_{28}$, 99 % purity, Fluka)
- n-Tetradecane (n-$C_{14}H_{30}$, 99 % purity, Fluka)
- n-Pentadecane (n-$C_{15}H_{32}$, 99 % purity, Fluka)
- Toluene (C_7H_8, 99.64 % purity, Fischer chemicals)

- Octanol ($C_8H_{17}OH$, 99.5 % purity, Unilab)

1.2.4 Quartz wool as the catalyst bed support (Alltech)

2. Equipments

The equipments used in this research were classified into 3 groups including (1) equipments for catalyst preparation, (2) instruments for catalyst characterization, and (3) equipments for Fischer-Tropsch synthesis reaction.

2.1 Equipments for Catalyst Preparation

2.1.1 Digital balance (AT 400, Metler Toledo)

2.1.2 Magnetic hot plate and stirrer (SLR, Schott)

2.1.3 Digital hot plate and stirrer (SLR, Schott)

2.1.4 Furnace (ELF10/6, Carbolite)

2.1.5 Hot air oven (ED53, Binder)

2.1.6 Desicator

2.1.7 Autoclave (made by order)

2.2 Equipments for Catalyst Characterization

2.2.1 Specific surface area, pore size distribution and pore volume

The specific surface area, pore volume, BJH pore diameter, and pore size distribution of the catalysts were determined by N_2 physisorption using a Quantachrome Autosorb-1C instrument at -196 ^oC. Prior to each measurement, samples were degassed at 200 ^oC for 12 h. The pore size distribution and pore volume were determined by BJH method and the specific surface area was estimated by BET method.

2.2.2 Transmission electron microscopy (TEM)

The structures of cobalt particles on monomodal and bimodal supports were revealed by transmission electron microscopy (JEOL JEM-2010 microscope with the acceleration voltage of 200 kV). The samples were prepared by suspending the sample in ethanol and followed by thermal evaporation of ethanol on a copper grid coated with a carbon film.

2.2.3 Thermogravimetric analysis and differential thermal analysis

The amount of weight loss and the temperature of cobalt precursor decomposition were investigated using the simultaneous TGA-DTA analyzer (SDT 2960 PN 925605.001, Perkin Elmer) in air at a heating rate of 10 ^{o}C/min. The samples weight used in each analysis was between 20 and 25 mg.

2.2.4 X-ray powder diffraction (XRD) spectroscopy

X-ray powder diffraction measurement was performed at room temperature using a Phillips powder diffractometer with monochromatized Cu-Kα radiation. Cobalt phases were detected by comparing the diffraction patterns with those of the standard powder XRD file compiled by the joint committee on powder diffraction standards (JCPDS) published by the International Center for Diffraction Data. The Co_3O_4 crystallite diameters were calculated by using Scherrer equation from the most intense Co_3O_4 peak at 2θ of 36.9 (as shown below).

$$d = \frac{0.89\lambda}{B\cos\theta} \times \frac{180^{o}}{\pi} \qquad (4)$$

where d is the mean crystallite diameter

λ is the X-ray wave length (1.54 Å)

B is the full width half maximum (FWHM) of the Co_3O_4 diffraction peak.

2.3 Equipments for Fischer-Tropsch Synthesis Reaction

2.3.1 Catalytic reaction testing unit

- Pressure regulator
- Mass flow controller (GFC117, Aalborg)
- Mass flow controller (8300 Series, KOFLOC)
- Thermocouple (K-type)
- Temperature controller (120-R/E, Shinho)
- Temperature indicator (RI, Shinho)
- Tube furnace (CFW 1300, Carbolite)
- Flexible heating tape (100 Volt)
- Voltage transformer (SB-5, SLIDEUP)
- Bubble flow meter

2.3.2 Gas analysis unit

- Gas chromatograph equipped with thermal conductivity detector (TCD) and chromatopac data processor (GC-2014, Shimadzu)
- Gas chromatograph equipped with flame ionization detector (FID) and chromatopac data processor (GC-8A, Shimadzu)
- Gas syringes (1002LTN Gastight Syringe, Hamilton and A-2 type Gastight Syringe, PS)
- Liquid syringe (80377 Microliter, Hamilton)

Experimental Procedures

In this research, the preparation of mesoporous silicas consisted of SBA-3, SBA-15 and bimodal mesoporous silica (BMS) were prepared at the first stage. After that, the cobalt support catalysts were prepared by incipient wetness impregnation (IMP) method and then the testing of Fischer-Tropsch synthesis performance was performed.

1. Methods of Mesoporous Silicas Synthesis

In order to synthesize the bimodal mesoporous silica from rice husk ash, prior to the mesoporous silica synthesis, rice husk ash-derived sodium silicate solution was firstly prepared (Chareonpanich *et al.*, 2004) and used as the silica source for bimodal porous silica preparation. The detailed procedures were as follows.

1.1 Preparation of Sodium Silicate from Rice Husk Ash

Sodium silicate solution ($Na_2Si_3O_7$: 4 wt. % NaOH: 27 wt. % SiO_2) was prepared from rice husk ash (RHA). First, 100 g of rice husk was refluxed with 1 L of 1 M HCl for 2.5 h. The treated rice husk was washed with distilled water, dried at 120 ^oC and burned in oxygen atmosphere at 700 ^oC for 1 h. The residual ash was composed of 99.7 wt. % amorphous silica.

Rice husk ash of 1.0 g was dissolved in 7.40 ml of 1 M NaOH solution and the obtained mixture was stirred at approximately 80 ^oC until clear solution was obtained. The volume of solution was one half decreased in order to obtain a desired composition of sodium silicate solution ($Na_2Si_3O_7$: 4 wt. % NaOH: 27 wt. % SiO_2) (Chareonpanich et al., 2004).

1.2 Synthesis of SBA-3 Mesoporous Silica

1.2.1 A solution of surfactant was prepared by stirring the mixture of 1 g of cethyltrimethyl ammonium bromide (CTAB) and 15 ml of hydrochloric acid in 47 ml of deinonized water at room temperature until the clear solution was obtained.

1.2.2 Then 4.45 ml of TEOS was dropwise added to the solution with vigorous stirring at 40^oC and the obtained mixture was kept stirring for 1 h.

1.2.3 The solid product was filtered and dried at 100 ^oC for 24 h and then calcined at 550 ^oC for 4 h to remove an organic template and volatile impurity.

1.3 Synthesis of SBA-15 Mesoporous Silica

The equipment set up in this experiment is shown in Figure 13.

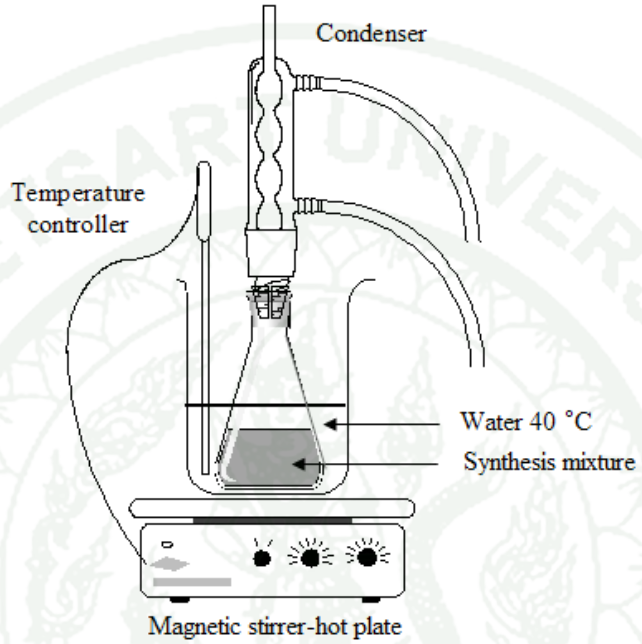

Figure 13 The equipment setup of hydrolysis and condensation process.

1.3.1 A solution of surfactant was prepared by stirring the mixture of 0.00875 mol (0.845 g) of Pluronic P123 and 60 ml of distilled water at room temperature until the clear solution was obtained.

1.3.2 Sodium silicate solution (based on one mole of silica) prepared from rice husk ash was added to Pluronic P123 solution and mixed properly.

1.3.3 After that, 4 mol of HCl solution (5.4 ml) was quickly added in the mixture under vigorous stirring at 40^{o}C and the obtained mixture was stirred for 24 h, from this stage of experiment the sol product was prepared.

1.3.4 The resulting sol was then transferred to a Teflon-lined autoclave and isothermally heated at 100 ^{o}C under autogeneous pressure for 24 h.

1.3.5 The solid product was washed with large amounts of warm distilled water and separated by mean of filtration.

1.3.6 The solid product was dried at 140 ^{o}C for 3 h and then calcined at 500 ^{o}C for 6 h to remove an organic template and volatile impurity. All of the steps can be summarized as shown in Figure 14.

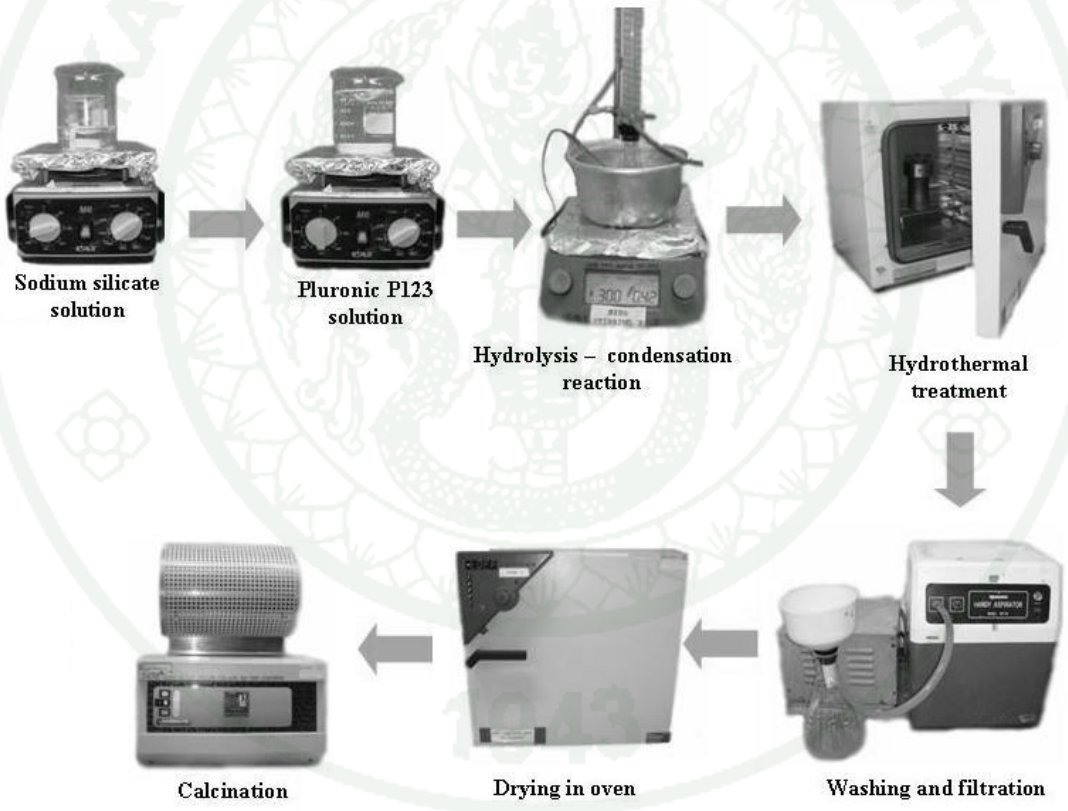

Figure 14 Scheme of SBA-15 mesoporous silica synthesis process.

1.4 Synthesis of Bimodal Mesoporous Silica

In this series of experiment, bimodal mesoporous silica products were synthesized using rice husk ash-derived sodium silicate and two kinds of templates including Pluronic P123 and CTAB was applied. An appropriate chemical composition of materials used for the synthesis of mesoporous silica SBA-15 at the molar ratio of SiO_2: Pluronic P123: HCl: H_2O of 1: 0.0875: 4: 200 was applied (Chareonpanich *et al*., 2007). The detailed procedures were as follows:

1.4.1 A solution of Pluronic P123 was prepared by dissolving 0.845 g of Pluronic P123 in 60 ml of distilled water under stirring at room temperature.

1.4.2 Sodium silicate based on 1g of silica was slowly added to the solution of Pluronic P123 and mixed properly under stirring (400 rpm) at 40 °C for 5 minutes. After that, 5.4 ml of HCl solution was rapidly added into the solution to begin the hydrolysis-condensation reaction. The obtained mixture was stirred at 40 °C for 24 h and the gel solution was formed.

1.4.3 Consecutively, CTAB and SiO_2 with mass ratios of 0.48; based on 1 g of additional SiO_2 were added separately to the gel solution. After that, 6.9 ml of HCl was rapidly added under stirring at 40 °C for 5 minute. The obtained gel solution was transferred to a Teflon-lined autoclave in which the hydrothermal aging was taken place at 100 °C for 24 h.

1.4.4 The solid product was collected by filtration, washed with distilled water, dried at 140 °C for 3 h, and calcined in air at 600 °C for 5 h. All of the step can be summarized as the schematic shown in Figure 15 and the detailed procedures were shown in Table 3.

Table 3 The detail mixing sequence of bimodal mesoporous silica synthesis during the hydrolysis-condensation stage

Sample	Hydrolysis-condensation stage – Sequence of mixing[a]		
	Stage-A1	Stage-A2	Stage-B
BMS-1	(P123+SS+HCl)-24 h	(CTAB+SS+HCl)-24 h	(A1+A2)-5 min
BMS-2	(P123+SS+HCl)-24 h	(CTAB+HCl)-5 min	(A1+A2)-5 min
BMS-3	(P123+CTAB)-5 min	(2SS+2HCl)-5 min	(A1+A2)-5 min

[a] The products from stage "B" was then performed hydrothermal aging at 100 °C for 24 h.

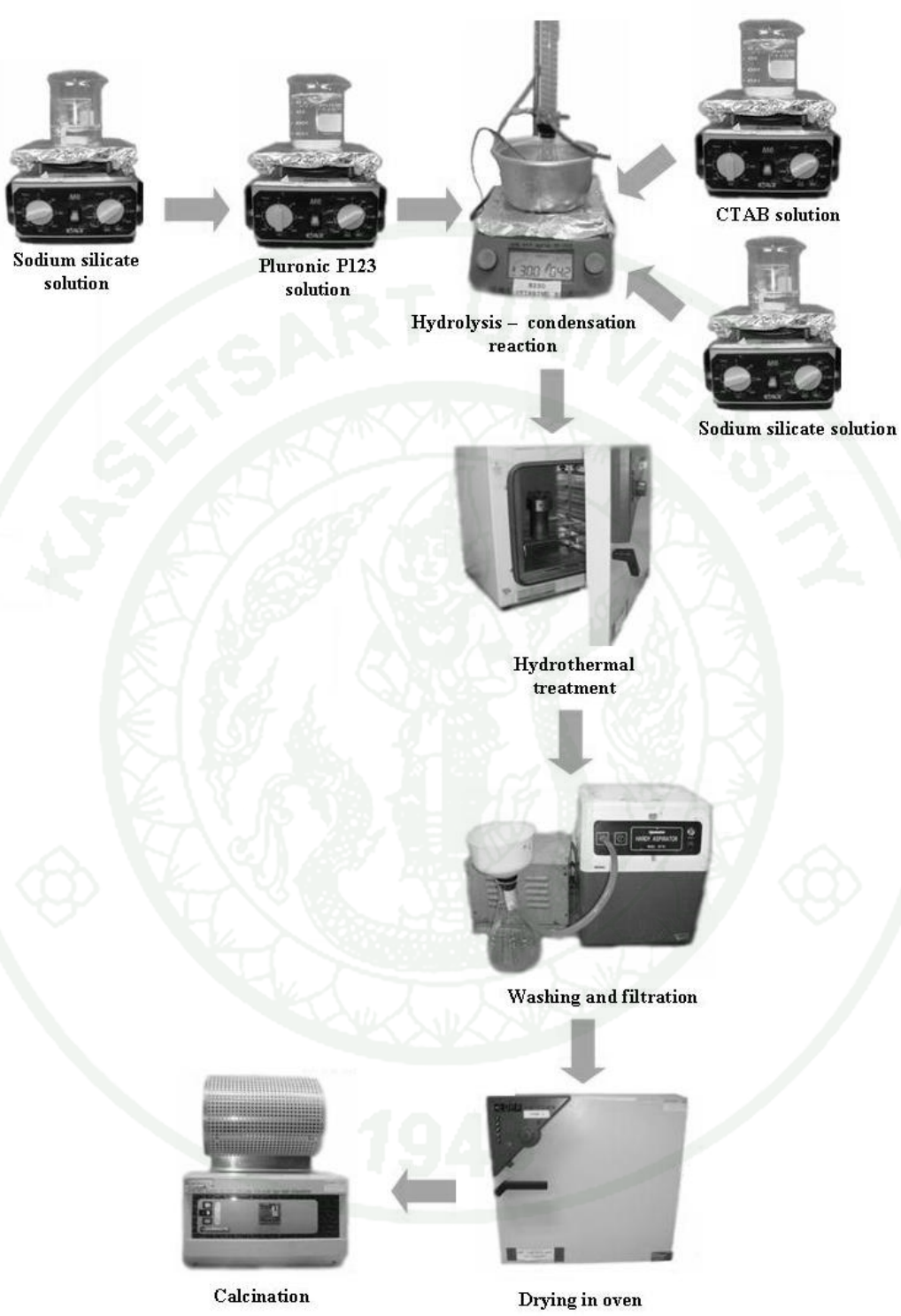

Figure 15 Scheme of bimodal mesoporous silica synthesis.

2. Preparation of Cobalt Supported Monomodal and Bimodal Mesoporous Catalysts

In this research, cobalt supported monomodal and bimodal porous catalysts (based on 5 wt.% loading) were prepared by wetness impregnation method. The monomodal and bimodal porous silicas used as the catalyst supports in this series of experiment were prepared by the process mentioned previously. The procedure of catalyst preparation was as follows:

2.1 The solution of metal precursor was prepared by dissolving certain amount of cobalt nitrate ($Co(NO_3)_2 \cdot 6H_2O$) in a required amount of distilled water under stirring.

2.2 The support of pellet size 0.2-0.3 mm was used and cobalt solution was slowly added into 1 g of supports (Figure 16).

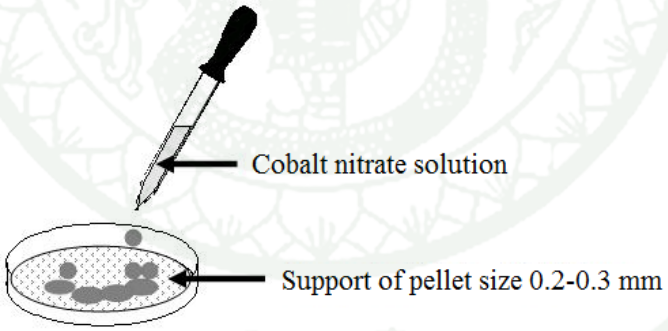

Figure 16 The stage of metal loading using wetness impregnation method.

2.3 The obtained mixture was dried at 120 °C for 24 h and calcined in air at 550 °C for 4 h.

The obtained catalyst granules were denoted as Co/SBA-3, Co/SBA-15, Co/BMS-1, Co/BMS-2, Co/BMS-3, respectively.

3. Performance Test of Fischer-Tropsch Synthesis

The catalytic testing unit for the Fischer-Tropsch synthesis reaction is shown in Figure 17. This experimental unit consists of a feed flow measuring and controlling system, a furnace equipped with stainless steel tube reactor and a sampling system. The catalytic reaction testing unit was designed to operate under high temperature and pressure conditions. The details of particular system are explained below.

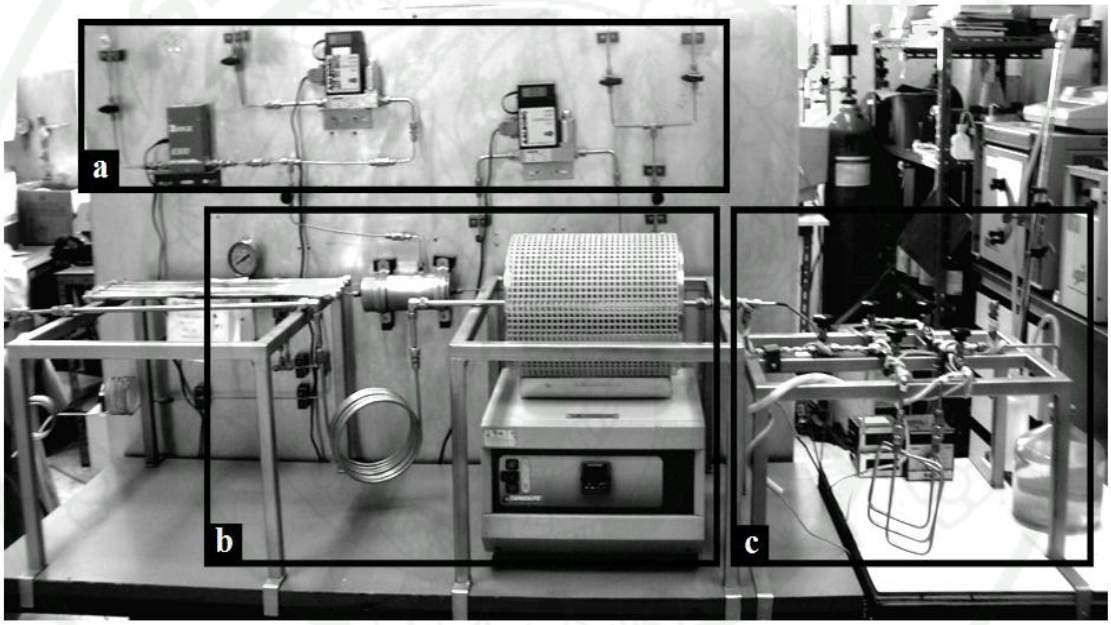

Figure 17 Catalytic reaction testing unit: (a) a feed flow measuring and controlling system, (b) a furnace-equipped stainless steel tube reactor and (c) a sampling system.

3.1 The Feed Flow Measuring and Controlling System

In this system, mass flow controllers were used to finely indicate and control the flow rate of feed gases including carbon monoxide, hydrogen, oxygen and nitrogen. Carbon monoxide and hydrogen were used as reactant gases, hydrogen was also used for the catalyst reduction, and oxygen was used for calcination process. In

order to monitor the system leakage, nitrogen gas was applied. Flow rates of hydrogen, oxygen and nitrogen were measured and controlled by Aalborg mass flow controller (Figure 18a) and KOFLOC mass flow controller (Figure 18b) was used to control the flow rate of carbon monoxide.

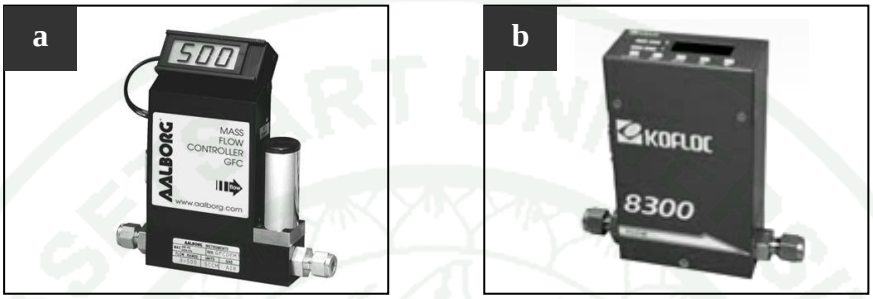

Figure 18 Mass flow controller: (a) Aalborg GFC thermal mass flow controller and (b) KOFLOC mass flow controller and mass flow meter with indicator.

3.2 The Packed Bed Reactor

The stainless steel tube was used as the packed-bed reactor. At the stage of reaction, the stainless steel tube was heated with an electric furnace (Figure 19) controlled by the temperature controller. A K-type thermocouple connected to a temperature controller unit was inserted inside the stainless steel tube in order to measure and control the temperature of the catalyst bed. Catalyst powder was packed in the isothermal zone of tube reactors between quartz wool layers as the scheme shown in Figure 20.

Figure 19 The Fischer-Tropsch synthesis reactor equipped with the electric heater (Carbolite tube furnace).

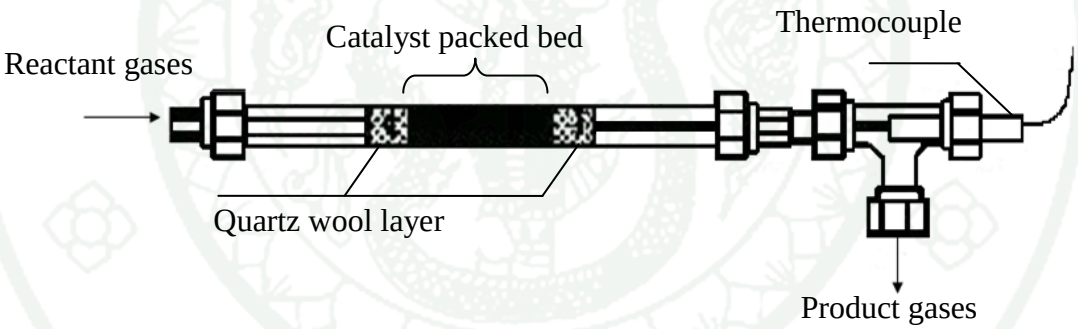

Figure 20 Schematic setup of the stage of Fischer-Tropsch reactor.

3.3 The Sampling System

The product gases were immediately sampled using a gas syringe from a heated sampling port connected to quick release valves, as shown Figure 21. Gas samples were analyzed by gas chromatographs. In the sampling unit, the sampling port, tube reactor and measuring valves were heated by heating tape to prevent gas condensation. The mixture of tail gas was trapped by water before venting to atmosphere and the exit flow rate was measured by a bubble flow meter.

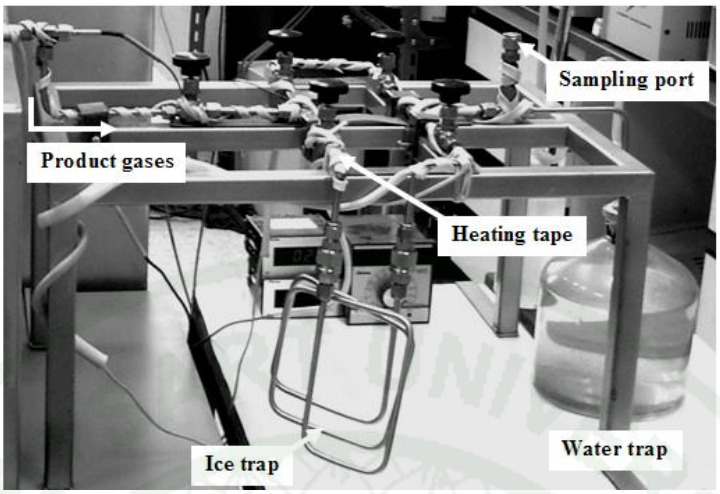

Figure 21 The sampling system consists of release valves, cooling trap, and sampling port heated by heating tapes and connected to bubble flow meter.

3.4 Gas Analysis Unit

Two types of gas chromatographs were applied to analyze the product gases. First, gas analysis unit (Figure 22) consists of Shimadzu gas chromatograph and chromatopac data processor (GC-2014) equipped with thermal conductivity detector (TCD) was used to quantitatively analyzed amounts of CO and CO_2 (Unibead-C packed column was applied).

Figure 22 Shimadzu gas chromatograph (GC-2014) equipped with thermal conductivity detector (TCD) and chromatopac data processor.

The conditions for CO and CO_2 analysis were:

- Initial carrier gas (He) flow rate 35 ml/min
- Final carrier gas (He) flow rate 60 ml/min
- Injector temperature 180 ^{o}C
- Initial column temperature 120 ^{o}C
- Final column temperature 200 ^{o}C
- Detector temperature (Pre) 200 ^{o}C
- Detector temperature 200 ^{o}C
- Current 80 mA

The amounts of hydrocarbon products (C_1-C_{15}) were analyzed by gas chromatograph (GC-8A, Shimadzu) equipped with flame ionization detector (FID) as shown in Figure 23. A Porapak-Q packed column (Shimadzu) and an OV-1 Uniport HP packed column (Shimadzu) were used to analyze C_1-C_4 hydrocarbons and C_5-C_{15} hydrocarbon, respectively. Helium (99.99 % purity) was used as the carrier gas, while hydrogen and air were used as the combustion gased for flame ionization detection.

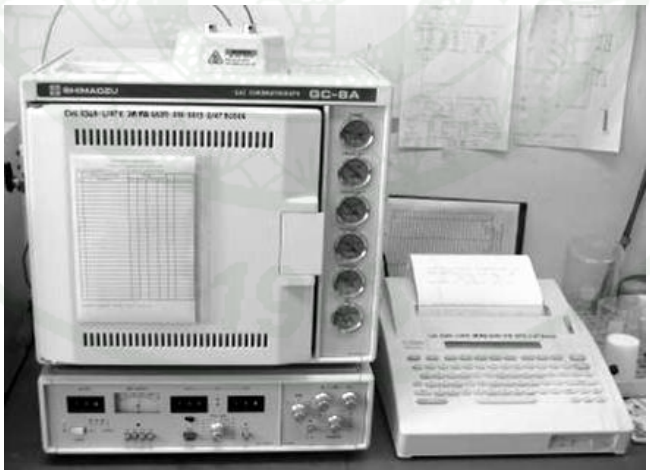

Figure 23 Shimadzu gas chromatograph (GC-8A) equipped with flame ionization detector (FID) and chromatopac data processor.

The conditions for C_1-C_4 hydrocarbons analysis were:

- Primary gas pressure	200	kPa (2 kg/cm^2)
- He carrier gas pressure	50	kPa (1 kg/cm^2)
- H_2 gas pressure	60	kPa (0.6 kg/cm^2)
- Air pressure	50	kPa (0.5 kg/cm^2)
- Injector/Detector temperature	230	^{o}C
- Column temperature	130	^{o}C
- Range	100	
- Attenuation	512	
- Analysis time	15	min

The conditions for C_5-C_{15} hydrocarbons analysis were:

- Primary gas pressure	200	kPa (2 kg/cm^2)
- He carrier gas pressure	100	kPa (1 kg/cm^2)
- H_2 gas pressure	60	kPa (0.6 kg/cm^2)
- Air pressure	50	kPa (0.5 kg/cm^2)
- Injector/Detector temperature	230	^{o}C
- Initial column temperature	30	^{o}C
- Final column temperature	230	^{o}C
- Temperature program rat	20	^{o}C/min
- Range	100	
- Attenuation	512	
- Holding time	5	min
- Analysis time	30	min

3.5 Test for FTS Perfermance

Before testing the catalyst performance, 0.5 g of cobalt supported catalyst was thoroughly mixed with 2 g of sand, in order to avoid the effect of poor heat transfer during catalyst testing experiment. The catalyst with sand was packed in stainless steel tube reactor (7.75 mm inner diameter, 0.89 mm wall thickness). To obtain an active form of catalyst, the catalyst was activated by reduction in H_2

atmosphere at 400 °C and 12 h at the flow rate of 60 ml/min (NTP) and then flushed and cooled with nitrogen. After pretreatment procedure, the catalyst was ready for the catalytic performance test.

During the reaction, CO and H_2 were converted to large ranges of hydrocarbon products over cobalt-containing monomodal and bimodal catalysts at a temperature of 220 °C with the CO/H_2 molar ratio of 1/2, total gas pressure of 10 atm and total gas flow rate of 60 ml/min, space velocity of syngas of 12 ml g^{-1} min^{-1}. Light and heavy hydrocarbon products were analyzed by gas chromatographs.

RESULTS AND DISCUSSION

In this present research, cobalt supported monomodal mesoporous silica (Co/SBA-3 and Co/SBA-15) and bimodal mesoporous silica (Co/BMS-1, Co/BMS-2 and Co/BMS-3) catalysts were prepared by incipient wetness impregnation methods based on 5 wt. % cobalt loading. The performances of the obtained catalysts were examined on the Fisher-Tropsch synthesis (FTS) reaction in order to investigate the effect of pore structure of these catalysts. The reaction conditions used in this stage were as follows: molar ratio of H_2/CO, 2; temperature, 220 ºC; total pressure, 10 atm; and total flow rate, 60 ml/min (NTP).

The experimental results and discussion were reported as the characteristics of cobalt supported monomodal and bimodal porous silica catalysts denoted as Co/SBA-3 and Co/SBA-15, and Co/BMS-X catalysts and their catalytic performances on FTS reaction, respectively. The physical and chemical properties of catalyst support and cobalt loaded catalysts were clarified and after that, the effect of pore structure on the catalyst activity and selectivity of FTS reaction were discussed.

1. Physical and Chemical Properties of Catalysts

In this part, the physical and chemical properties of cobalt supported catalysts were investigated by using N_2-sorption measurement, XRD analysis, SAXS analysis and TEM technique. The detail of results is shown below.

The physical properties of the supports (SBA-3, SBA-15 and BMS-Xs) and the cobalt catalysts (Co/SBA-3, Co/SBA-15 and Co/BMS-Xs) are listed in Table 4. It can be clearly seen that when the silica supports were impregnated with Co ions by using cobalt (II) nitrate solution as a metal precursor, the total pore volume and specific surface area of all catalysts were decreased. In the case of monomodal porous silica catalysts the specific surface area were sharply decreased from 1,440 m^2/g to 630 m^2/g (56%) for Co/SBA-3 and 569 m^2/g to 385 m^2/g (37%) for Co/SBA-

15, respectively. In the case of bimodal porous silica catalysts, the specific surface area was decreased from 707 m^2/g to 435 m^2/g (38%) for Co/BMS-1; 662 m^2/g to 451 m^2/g (32%) for Co/BMS-2 and 955 m^2/g to 494 m^2/g (48%) for Co/BMS-3. The largest decrease of the seen that the specific surface area was found with Co/SBA-3 with smallest pore diameter of 2.4 nm (56%). In the case of bimodal mesoporous silica catalyst, the similar BET surface area changes were found and this value was close to that of the Co/SBA-15 (37%). This could be attributed to the strong effect of large pores size of SBA-15 in the bimodal mesoporous silica catalysts. However, it was observed that the decreases of the specific surface area of Co/BMS-3 catalyst had the different trend from other bimodal porous silica catalysts and it was similar to that of the Co/SBA-3. It could be explained that with the BMS-3 support, the cluster of cobalt supported smaller pore SBA-3 like silica, surrounding by larger pores formed as the inter-cluster channels (as show in Figure 28(e)) were found. As a result, similar result to that of Co/SBA-3 catalyst was observed.

The decreases of specific surface area and pore volume were caused by pore blocking as a result of the loaded cobalt species, as was also found by Vinu *et al.*, (2008) and Shah *et al*., (2007). By using the incipient wetness impregnation methods, cobalt oxides often formed in the pore channels and/or on the external surfaces of the support. Cobalt oxides formed in the mesopores could partially or fully block the pore channels, resulting in pore inaccessible for nitrogen adsorption, and therefore reducing the surface area and pore volume of the catalysts.

Table 4 BET surface area, pore volume and pore diameter of mesoporous silicas and cobalt loaded mesoporous silicas.

Sample	BET surface area (m^2/g)	Pore volume (cm^3/g)	Pore diameter (nm)
SBA-3	1440	1.1	2.4
SBA-15	569	0.9	6.5
BMS-1	707	1.0	3.8, 6.5
BMS-2	662	0.9	3.8, 6.5
BMS-3	955	1.5	3.4, 12.2
Co/SBA-3	630	0.7	2.4
Co/SBA-15	358	0.6	3.8, 6.5
Co/BMS-1	435	0.7	3.8, 6.5
Co/BMS-2	451	0.9	3.8, 6.5
Co/BMS-3	494	1.3	4.2

The N_2 adsorption-desorption isotherms at 77 k of the silica supports and cobalt supported catalysts are presented in Figure 24. In all cases, the type IV isotherms indicating the existence of mesoporous materials classified by IUPAC were observed and revealed H1 hysteresis loop as the capillary condensation was occurred. As shown in Figure 24 (a), the BMS-3 bimodal mesoporous silica provided the H1 hysteresis loop consisting one capillary condensation step at P/P_o of 0.65-0.95, whereas the other products including BMS-1, and BMS-2 exhibited independent and intricately interweave mesopore structures with two capillary condensation steps in the P/P_o ranges of 0.45-0.65 and 0.65-0.95. In the case of cobalt supported catalysts, the shapes of N_2 adsorption-desorption isotherms for all the catalysts were similar to that of the original SBA-3, SBA-15 and BMS-X supports (as shown in Figure 24(b)). It implied that the mesoporous structure of the silica supports were mostly retained upon cobalt impregnation.

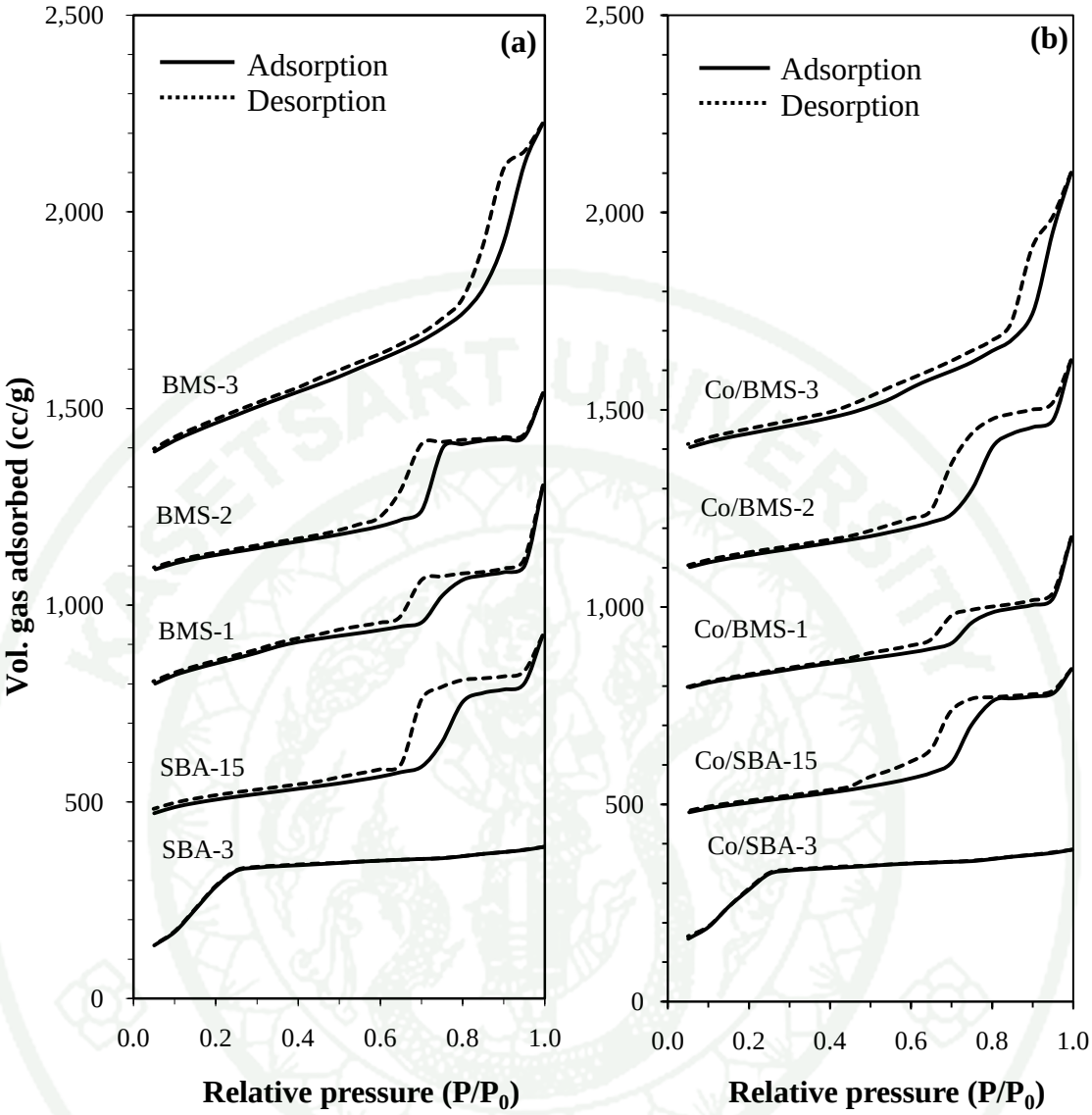

Figure 24 N_2-sorption isotherms of (a) mesoporous silica (b) cobalt loaded mesoporous silica. The sorption isotherms were shifted by 0, 400, 700, 1,000 and 1,300 cc/g, corresponding to the lowest and the highest values of volume of gas adsorbed.

The BJH pore size distribution curves of mesoporous silica supports and cobalt supported catalysts are shown in Figure 25. The monomodal mesoporous silica supports of smaller pore (SBA-3) and larger pore (SBA-15) presented one pore size distribution of 2.4 and 6.5 nm, respectively. The bimodal mesoporous silica supports the BMS-1 had the main pore size at 6.5 nm and few of pores at 2.7 and 3.8 nm,

whereas BMS-2 revealed sharp pore size distribution at mean pore size of 6.5 nm. On the other hand, as its characteristics of smaller pore occurred in larger pore, BMS-3 product showed wide pore size distribution (PSD) with pore sizes ranging from 2 to 17 nm. As shown in Figure 25(b), the PSD patterns of pore size distribution for the cobalt catalysts were similar to that of original monomodal and bimodal mesoporous silica supports, but their peak intensities were obviously smaller than those of pure mesoporous silica supports. It should be noted that the pore diameter was not change due to insignificant effect of cobalt loading on quite large pore diameters of SBA-15 (6.5 nm) and the series of BMS-X supports of which contained larger pore of SBA-15. This observation was in good agreement with the results reported by Khodakov *et al.,* (2005) that revealed a less impact on the long range order of mesoporous silica support occurred by the aqueous impregnation on SBA-15.

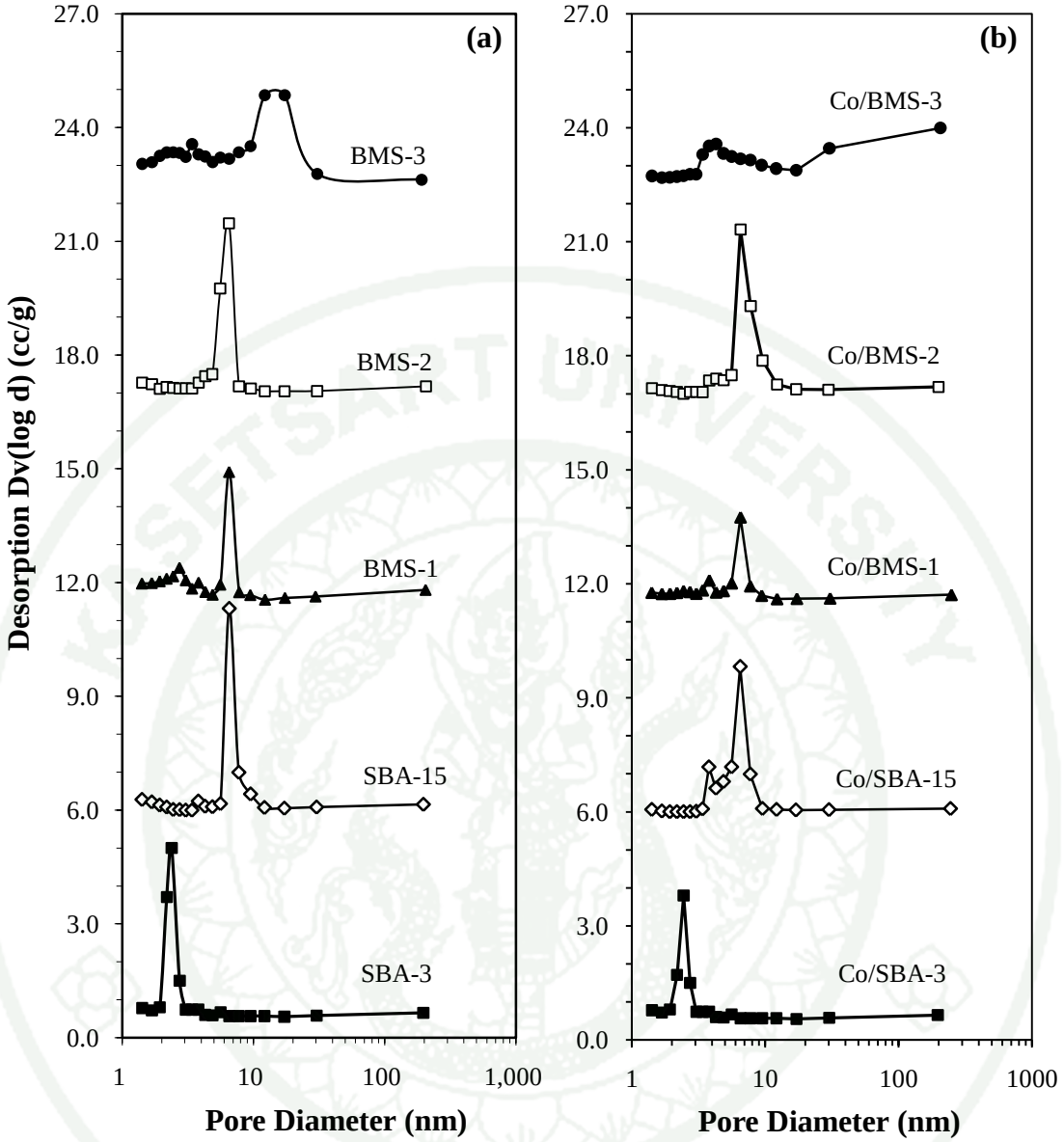

Figure 25 BJH pore size distribution curves from nitrogen desorption isotherms for (a) silica (b) cobalt loaded mesoporous silica. The pore size distributions were shifted by 0.5, 6.5, 11.5, 17.5 and 22.5 cc/g, corresponding to the lowest and highest values of volume of gas adsorbed.

In addition, the small peaks at the position around 4 nm are clearly observed in both the calcined SBA-15 silica support and Co/SBA-15 catalysts (Figure 25); these the mentioned samples exhibited the same behavior of which could be attributed

to the formation of silica xerogel from incomplete hydrolysis-condensation reaction during the micelle-templating stage in the SBA-15 synthesis process. During the sol-gel process, unhydrolyzed silica species could form as small particles of amorphous silica and incorporated with the completely hydrolyzed silica network in the synthesis mixture (Dunn *et al.*, 2004). When the solvent was evaporated in the drying process, unhydrolyzed silica particles could agglomerate (silica xerogel) and retained high porosity with small pore size (smaller than the pore size of SBA-15 support) within the entire catalyst structure.

In the small angle region of SAXS (Figure 26), the as-synthesized BMS-1 and BMS-2 presented the major peaks at 2θ of 0.87 and 0.90, respectively. These revealed the main pore size of BMS-1 and BMS-2 products, whereas the smaller peaks at 2θ of 1.53-1.55 and 1.75-1.78 could confirmed the ordered 2D-hexagonal structures of SBA-15 in the BMS products. In the case of BMS-3, the smaller peaks of SAXS pattern were disappeared and the major peak was shift to lower 2θ, these results confirmed the disordered 2D-hexagonal structure and the larger pore size of mesoporous silica cluster formed by the aggregation of mesoporous primary nanoparticles, respectively. With the 5 wt.% Co loading in the Co/BMS-X catalysts, the SAXS profiles were almost unchanged and exhibited the highly diffraction peaks at low 2θ, reflecting the ordered structure of BMS-1, BMS-2 and BMS-3. It was evident that the structures of the calcined BMS-X products were still retained to some extent even by adding 5 wt.% cobalt. However, it was found that after Co loading, the intensity of the major peaks of each catalyst gradually decreased and the peak became broader. It implied that BMS-1, BMS-2 and BMS-3 could possibly partially collapsed during calcinations and Co loading.

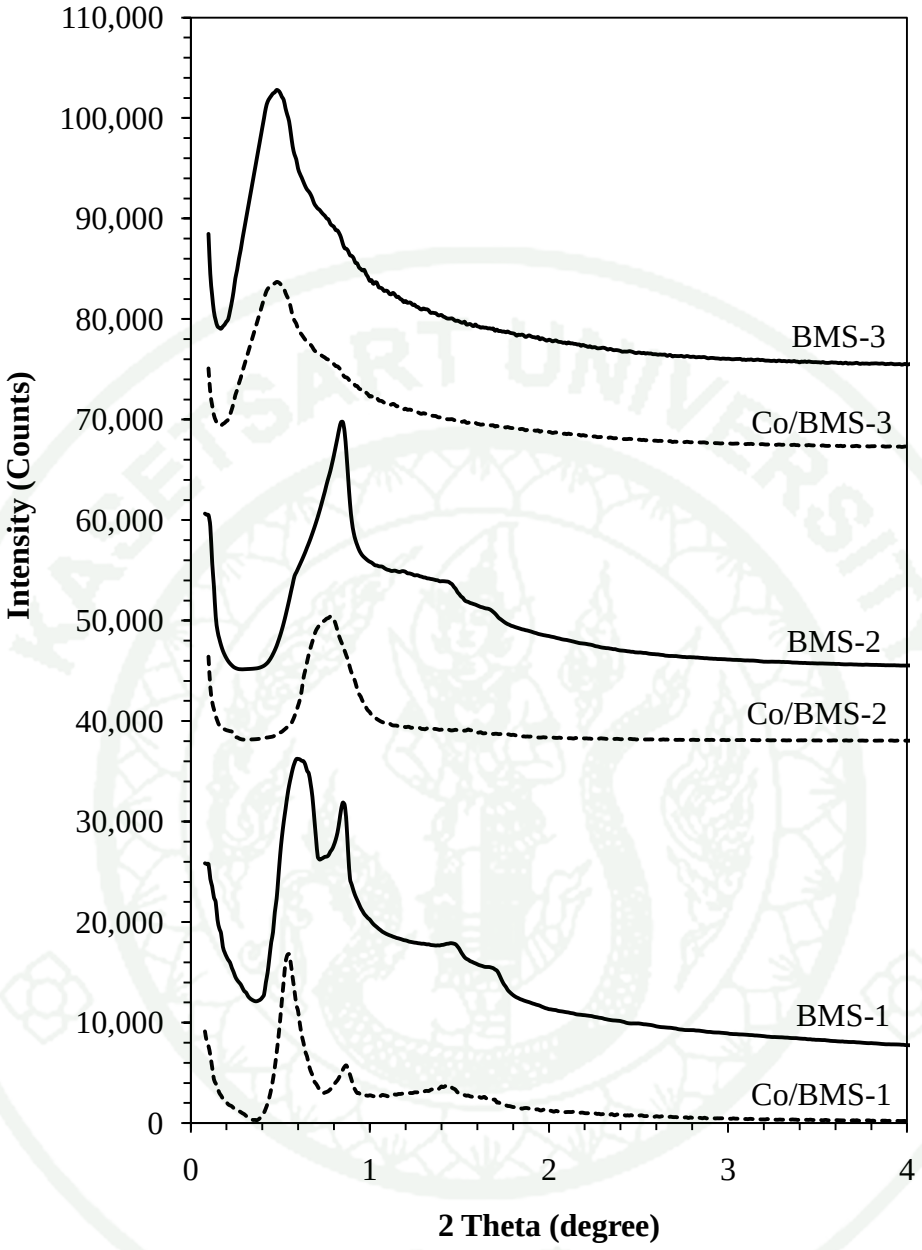

Figure 26 Small angle X-ray scattering (SAXS) patterns of bimodal mesoporous silicas (BMS-X) before and after 5 wt.% cobalt loading**.** The X-ray scattering patterns were shifted by 0, 7,000, 35,000, 42,000, 63,000 and 70,000 counts, corresponding to the lowest and highest values of intensity.

X-ray diffraction analysis was performed in order to investigate the types of cobalt species and average Co_3O_4 crystallite size. As shown in Figure 27, all catalysts mainly composed of Co_3O_4 spinel phase with 2θ of 31.3, 36.9, 44.8, 59.4 and 65.3, indicated that after calcinations cobalt species were presented in the form of crystalline Co_3O_4 spinel on all types of catalysts. No other crystalline phase was detected on the prepared cobalt supported catalysts after calcination. For Co/SBA-3 catalyst, it was found that the intensity of the corresponding peaks was lower than that of the other Co catalysts; this was due to the fact that cobalt species in Co/SBA-3 catalyst were highly dispersed on the SBA-3 surface. The crystallite sizes of Co_3O_4 calculated by using Scherrer equation were listed in Table 5. It was found that the Co_3O_4 crystallite size was increased with increasing the mesopore diameter. Similar trend was also reported by Song *et al.,* (2006). In the case of Co/SBA-3, the Co_3O_4 crystallite size was smallest due to the small pore size of SBA-3 support. However, it was clearly observed that the Co_3O_4 crystallite sizes of BMS-1 and BMS-2 were close to that of the Co/SBA-15 catalyst. This could be due to the large pores size of SBA-15 ramdomly distributed in the bimodal mesoporous silica catalyst of which strongly affect the Co particle size formed on the surface of these catalysts.

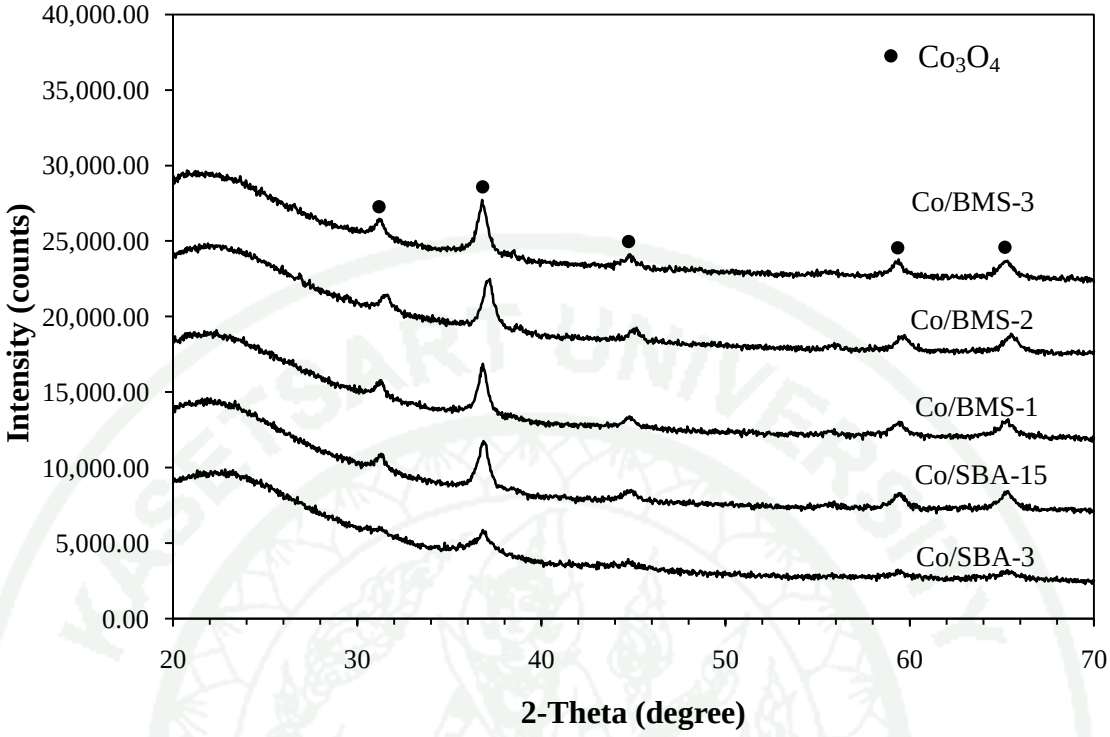

Figure 27 XRD patterns of calcined cobalt supported silica catalysts. The X-ray scattering patterns were shifted by 0, 5,000, 10,000, 15,000 and 20,000 counts, corresponding to the lowest and highest values of intensity.

Table 5 Average Co_3O_4 crystallite diameter of cobalt supported catalysts with different pore structures of silica supports.

Catalysts	Co_3O_4 crystallite diameter [a] (nm)
Co/SBA-3	6.9
Co/SBA-15	12.0
Co/BMS-1	13.6
Co/BMS-2	12.5
Co/BMS-3	14.2

[a] Mean diameter of Co_3O_4 crystallite determined by XRD (Scherrer equation).

TEM analysis was performed to investigate the shape and morphology of supports and the aggregates of Co_3O_4 crystal on supports. As shown in Figure 28, the darker spots (arrow 1) on the catalyst granules represent an area of high concentration of Co_3O_4, whereas the other parts (arrow 2) indicate the silica support with minimal or no Co_3O_4 presented. It can be clearly seen that, in the case of monomodal mesoporous silica catalysts (Figure 28(a) and (b)) the Co_3O_4 crystallite size of Co/SBA-3 (Figure 28(a)) was smaller than that of Co/SBA-15 (Figure 28(b)) and presented areas with high density of cobalt crystallites. The dark areas of Co/SBA-3 give a smeared contrast over the channels, which correspond to cobalt oxide particles on the external surface. Moreover, the cobalt oxide particles in Co/SBA-3 are presented as the cobalt clusters.

In the case of bimodal mesoporous silica catalysts (Co/BMS-X catalysts) which containing smaller pore of SBA-3 and larger pore of SBA-15, two different sizes of Co particle were obtained. The phase separation morphology between SBA-3 and SBA-15 of Co/BMS-1 was clearly observed from TEM image (Figure 28(c)). It was found that the Co_3O_4 crystallite sizes were smaller and more dispersed in the phase of SBA-3 whereas they were larger with less dispersed in the phase of SBA-15.

In the case of the Co/BMS-2 (Figure 28(d)), it was obviously seen that the thoroughly mixed phases between SBA-3 and SBA-15 were observed. With the Co/BMS-2 catalyst Co particles mainly dispersed in larger pores of SBA-15 and some of smaller Co particles dispersed in smaller pores of SBA-3. It was probably because cobalt nitrate solution hardly diffuse into small pores of SBA-3 that infiltrated in SBA-15 mesoporous silica. As a result, the Co/BMS-3 catalyst with high Co dispersion on the surface was observed (as shown in Figure 28(e)).

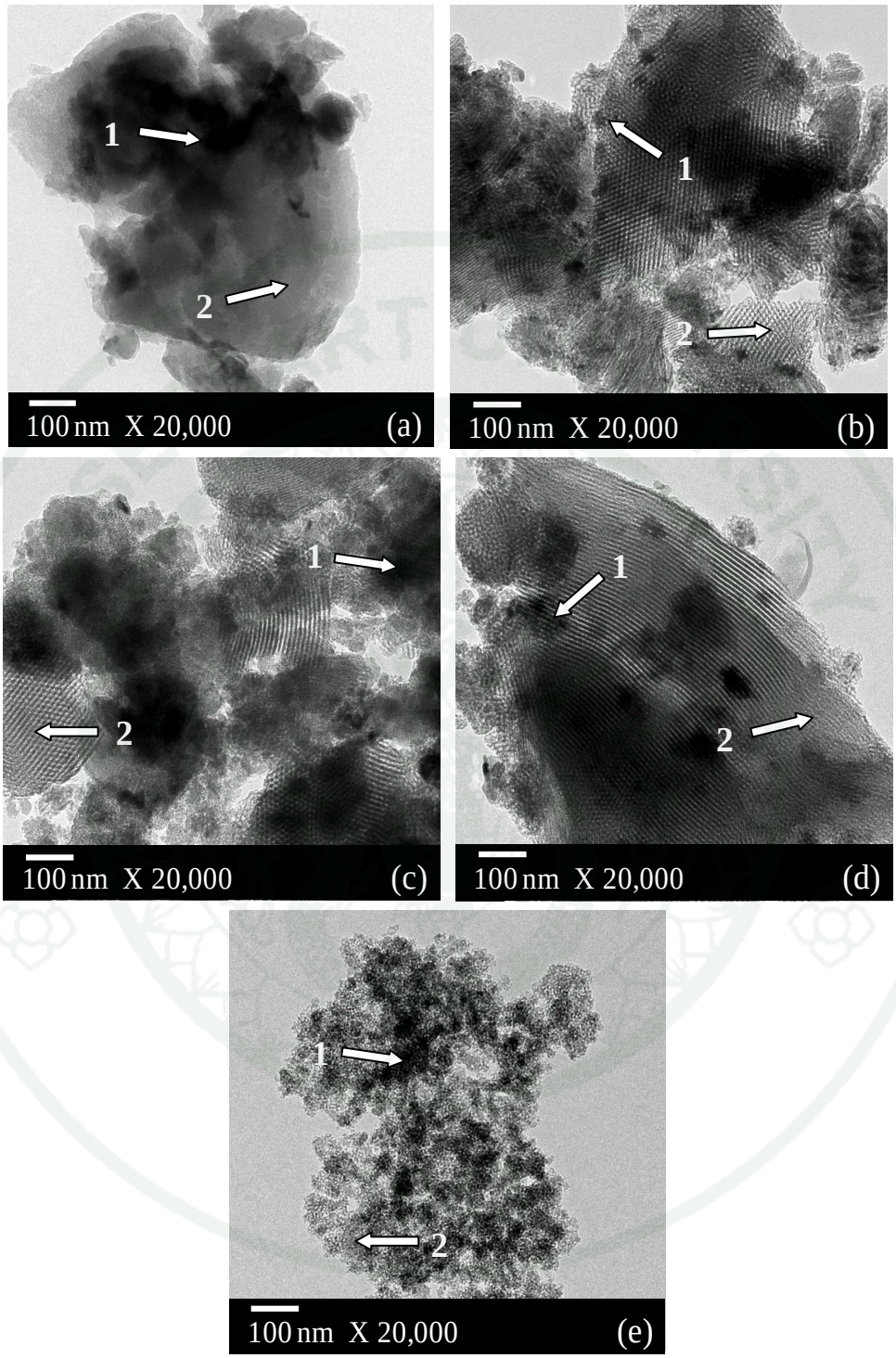

Figure 28 TEM micrographs of cobalt supported catalysts: (a) Co/SBA-3 (b) Co/SBA-15 (c) Co/BMS-1 (d) Co/BMS-2 (e) Co/BMS-3. Arrow 1 representing the area of high concentration of Co_3O_4, and arrow 2 representing the silica support with minimal or no Co_3O_4 presented.

2. Investigation of Catalytic FTS Performance

The testing of FTS catalytic performance was carried out in order to clarify the effect of pore structures on the catalytic behavior of 5 wt.% cobalt supported catalysts. Each catalyst obtained from the previous synthesis stage was reduced before the FTS performance test at 400 °C for 12 h. The catalytic FTS activities of different cobalt supported catalysts were studied in a packed-bed reactor at the H_2/CO molar ratio of 2/1, the total flow rate of 60 ml/min (NTP) and total pressure of 10 atm. The reaction temperature was fixed at 220 °C (This reaction temperature was selected according the previous work done by Prieto *et al*., 2009. Before the FTS reaction, reactant gases temperature was slowly increased from room temperature to 220 °C using the heating rate of 5 °C/min and this temperature rising program was applied throughout the study to avoid the deactivation of catalysts (Afonso *et al.*, 1997).

In this series of experiment, in order to study the effect of the pore structures on the catalyst performances and catalytic behaviors, the activity and selectivity towards heavy hydrocarbon (C_{5+}) over bimodal mesoporous silica catalysts (Co/BMS-X catalysts) prepared by incipient wetness impregnation method were compared to those of monomodal porous silica catalysts (Co/SBA-3 and Co/SBA-15). The results of the performance FTS over 5 wt.% cobalt catalysts are shown below.

2.1 Activities of the catalysts

The results of CO conversion and product distribution of cobalt supported monomodal and bimodal pores silica catalysts prepared by incipient wetness impregnation technique are presented in Table 6.

Table 6 CO conversion and product distribution of catalytic FTS reaction obtained over Co supported monomodal and bimodal pores silica catalysts.

Catalyst*	CO conversion (%)	Hydrocarbon selectivity (wt.%)				
		C_1	C_2	C_3	C_4	C_{5+}
Co/SBA-3	8.2	30.6	2.0	5.3	2.7	60.5
Co/SBA-15	9.7	20.1	1.4	4.8	3.1	70.4
Co/BMS-1	14.3	12.7	1.3	4.3	2.1	81.7
Co/BMS-2	12.1	21.3	2.2	7.0	4.9	60.5
Co/BMS-3	7.5	22.5	2.4	7.1	3.8	67.0

*All the catalysts were reduced in the flow of H_2 at 400°C for 12 h before FTS reaction.

Reaction conditions: H_2/CO = 2/1; temperature, 220°C; pressure, 10 bar; flow rate, 60 ml/min (NTP), space velocity = 12 ml $g^{-1}min^{-1}$.

As shown in Table 6, the bimodal mesoporous silica catalysts (Co/BMS-1 and Co/BMS-2) were more active than monomodal mesoporous silica catalysts (Co/SBA-3 and Co/SBA-15). The Co/BMS-1 catalyst with small and large pore diameters formed from the phase separation between SBA-3 and SBA-15, respectively, presented the highest CO conversion (14.3%) among all the catalysts. This CO conversion was relatively higher than these of 5 wt.% cobalt loading on the other supports as previously shown in Table 2. With Co/SBA-3 and Co/SBA-15 catalysts, significantly low CO conversions of 8.2% and 9.7%, respectively, were found when compared to those of Co/BMS-1 and Co/BMS-2 catalysts. In the case of Co/SBA-3, this could be attributed to small particle size of cobalt metal formed on SBA-3 surface of which easily reoxidized by water and other reaction products and thus become inactive during the FTS reaction. In the case of bimodal mesoporous silica catalysts with small and large pore diameters, a greater amount of Co^0 active surface could be formed. Moreover, it was clearly seen that Co/SBA-3 catalyst had higher selectivity towards methane and low heavy hydrocarbons (C_{5+}) selectivity than

bimodal mesoporous silica catalysts. The difference in selectivities of Co/SBA-3, Co/SBA-15 and Co/BMS-X were explained as follows:

As Co/BMS-1 catalyst exhibited the highest activity (14.3 % CO conversion) in FTS reaction (as shown in Table 6), this could be due to the support structure of which containing small and large pore diameter occurred by phase separation between SBA-3 and SBA-15. As a result, a greater amount of Co^0 active surface was obtained. In the case of Co/BMS-2 catalyst, the activity (12.1 % CO conversion) was a little lower than that of the activity of Co/BMS-1. This could be attributed to the structure of Co/BMS-2 catalyst having two pore-size diameters similar to these of the Co/BMS-1 catalyst. However, it was found that Co/BMS-3 catalyst gave the lowest CO conversion (7.5 %), whereas other Co/BMS-X catalysts revealed the higher avtivity when compare to the monomodal porous silica catalysts. It could be explained that with the BMS-3, the cluster of smaller pore SBA-3 like silica cobalt supported, surrounding by larger pores formed as the inter-cluster channels (as show in Figure 28(e)) were found. As a result, similar result to that of Co/SBA-3 catalyst was observed.

Indeed, the suggested mechanism of FTS reaction was regarded as a surface-catalyzed polymerization process. The reaction of CO hydrogenation was taken place over the cobalt supported catalyst surface. The mechanism began with the adsorption of CO and H_2 molecules on cobalt active sites (Equation 5) and the dissociation of H_2 (Equation 6) and CO (Equation 7) were further occurred. The hydrogenation of adsorbed C species was then performed, resulting in the CH_x monomers which were further polymerized to larger hydrocarbon products (Iglesia, 1997; Davis, 2001 and Burton, 2001). These mentioned mechanisms were shown as follows:

$$CO + S_{Co} \longrightarrow CO\text{-}S_{Co} \qquad (5)$$

$$H_2 + S_{Co} \longrightarrow 2H\text{-}S_{Co} \qquad (6)$$

$$CO\text{-}S_{Co} + S_{Co} \longrightarrow C\text{-}S_{Co} + O\text{-}S_{Co} \quad (7)$$

Where S_{Co} is cobalt active site.

$C\text{-}S_{Co}$ is adsorbed carbon on cobalt active site.

$O\text{-}S_{Co}$ is adsorbed oxygen on cobalt active site.

$H\text{-}S_{Co}$ is adsorbed hydrogen on cobalt active site.

$R\text{-}S_{Co}$ is adsorbed hydrocarbon products on cobalt active site.

The reaction between adsorbed carbon species and adsorbed hydrogen species were occurred and followed by the chain propagation as the following equations:

$$C\text{-}S_{Co} + H\text{-}S_{Co} \longrightarrow CH\text{-}S_{Co} + S_{Co} \quad (8)$$

$$CH\text{-}S_{Co} + CH\text{-}S_{Co} \longrightarrow R\text{-}S_{Co} + S_{Co} \quad (9)$$

Finally, the chain termination occurred as shown in Equation 10:

$$R\text{-}S_{Co} \longrightarrow R + S_{Co} \quad (10)$$

It is well-known that the FTS activity of supported cobalt catalyst strongly depends on the number of cobalt active sites after reduction and directly related to the reduction degree (Liu *et al.*, 2007). In addition, cobalt particle size is a key factor affecting the cobalt reducibility. According to TEM images of Co/SBA-15 catalyst (Figure 28), it was clearly shown that cobalt species agglomerated to form large cobalt particles on the silica surface. The TEM image of Co/BMS-1 and Co/BMS-2 exhibited the smaller Co particles formed on the small pore of SBA-3 portion, whereas larger Co particles formed on the large pore of SBA-15 portion. The agglomeration of cobalt metals was attributed to the weak interaction between silica and cobalt precursor (Liu *et al.*, 2007). As a result, Co/SBA-15, Co/BMS-1 and Co/BMS-2 catalysts having large cobalt particles revealed higher extent of cobalt reduction (Girardon *et al.*, 2007). In the case of Co/SBA-3, smaller particle size of

cobalt metals was formed on SBA-3 surface of which hardly reduced to form active Co^0, however easily reoxidized by water and other reaction products and thus become inactive during the FTS reaction.

In general, for cobalt catalysts supported on silica, two-stage reduction was observed; Co_3O_4 was reduced to CoO and then to metallic (Co^0). It could be ascribed to the successive reduction of Co_3O_4 to CoO at the step temperature around 300 °C and the subsequent reduction of CoO to metallic Co at around 550 °C (Steen *et al.,* 1996) as shown in Equations (11) and (12), respectively:

$$Co_3O_4 + H_2 \longrightarrow 3CoO + H_2O \qquad (11)$$

$$CoO + H_2 \longrightarrow Co + H_2O \qquad (12)$$

Furthermore, the FTS activity of cobalt supported catalyst was also related to the particular surface property of catalyst. Large cobalt particles provided large flat metallic surface, favoring bridge-type adsorbed CO (Zhang *et al.,* 2007). The large cobalt particles of Co/SBA-15 catalyst were more easily to form the bridge-type CO during the FTS reaction compared to the small cobalt particles of which favored the formation of linear-type CO on active metals (Jalama *et al.,* 2007). Accordingly, Co/SBA-15 catalyst with large cobalt particles greatly promoted the bridge-type CO formation than the linear-type CO of which preferably obtained from the smaller cobalt particles. The bridge-type CO had a weaker C–O bond and thus could be more easily dissociated to carbon and oxygen, which was one of the crucial processes in FTS reaction (Xiong *et al.,* 2008).

Consequently, the lower activity of Co/SBA-3 catalyst was attributed to the smaller cobalt particles. The stronger interaction between cobalt species and the silica support resulted in the lower reducibility of cobalt metal, resulting in the lower amount of Co^0 active sites (Girardon *et al.,* 2007).

Furthermore, the FTS activity of cobalt supported catalyst was also related to the temperature that use in reaction.

Table 7 CO conversion and product distribution of Co catalysts under different temperature conditions

Temp. (ºC)	Catalyst	X_{CO}[a] (%)	Hydrocarbon selectivity (wt.%)				
			C_1	C_2	C_3	C_4	C_{5+}
180	Co/SBA-3	2.7	24.2	1.6	3.4	2.7	77.2
	Co/SBA-15	3.9	9.6	1.3	2.6	1.8	85.2
	Co/BMS-1	5.8	6.2	1.0	1.6	1.6	89.6
	Co/BMS-2	4.7	11.2	1.1	2.3	1.1	86.1
	Co/BMS-3	3.4	13.8	1.1	2.4	1.6	81.2
200	Co/SBA-3	5.2	27.4	1.8	4.5	2.0	67.9
	Co/SBA-15	6.6	14.0	1.9	3.2	2.7	78.2
	Co/BMS-1	9.2	10.1	1.1	2.7	2.6	84.9
	Co/BMS-2	8.1	14.9	1.2	3.8	1.4	78.7
	Co/BMS-3	5.1	17.3	1.3	4.7	2.0	75.1
220	Co/SBA-3	8.2	30.6	2.0	5.3	2.7	60.5
	Co/SBA-15	9.7	20.1	1.4	4.8	3.1	70.4
	Co/BMS-1	14.3	12.7	1.3	4.3	2.1	81.7
	Co/BMS-2	12.1	21.3	2.2	7.0	4.9	60.5
	Co/BMS-3	7.5	22.5	2.4	7.1	3.8	67.0

[a] CO conversion

At the FTS temperature of 180 ºC, the CO conversions of all the catalysts were quite low (in the range of 2.7%-5.8%). It was suggested that the lowest CO conversion and also the lowest methane selectivity were obtained at this temperature which the C_{5+} selectivity was highest for all catalysts was still present.

The results at 200 ºC showed that the value of CO conversions were significantly increase from the CO conversion at 180 ºC. As shown in Table 7, the CO conversion in the range of 5.1%-9.2% was obtained from all cobalt supported pores silica catalysts, the C_{5+} selectivity was decreased at this temperature while methane selectivity increased.

Similarly to the result at 200 ºC, at 220 ºC the highest CO conversions in the range of 8.5-14.5 % were obtained. In this case, the highest methane selectivity (30.6 %) and the lowest C_{5+} selectivity (60.5 %) were formed. It should be mentioned that among all the catalysts used in this study, Co/SBA-3 catalyst gave the highest methane and the lowest C_{5+} selectivities. This could be attributed to the smaller pore diameter of support, resulting in the high cobalt dispersion with small Co particle size in this catalyst.

In the case of Co/BMS-1 catalysts, the highest selectivity of C_{5+} compared to other catalysts was found. It may be due to the pore structure of this catalyst must be suitable to promote the formation of long-chain hydrocarbons than other monomodal and bimodal pores structures. In the case of monomodal mesoporous silica catalyst, Co/SBA-3 the lowest C_{5+} selectivity was observed in all case, this could be attributed to the effect of the smallest pore size of this catalyst resulting in smallest cobalt particle size of which revealed less reducibility to form active Co^0 metal.

The increase of the reaction temperature resulted in an increase in methane and C_2-C_4 selectivities (light hydrocarbons) and CO conversion, whereas C_{5+} selectivity was decreased (as shown in Table 7). At higher reaction temperatures, olefins were preferentially hydrogenated and chain propagation was suppressed. The higher operating temperature resulted in a shift in selectivity towards lower carbon number products (low α) and more hydrogenated products (Dry, 2002). A number of studies revealed that the influence of the increase of reaction temperature showed the higher methane selectivity on the cobalt catalysts (Bachara *et al*., 2001; Das *et al*., 2003; Hurlbut *et al*. 1996; and Rohr *et al*., 2000). However, the study of carbon

monoxide hydrogenation on cobalt supported alumina revealed that the higher reaction temperature would cause an increase in hydrogenation activity, resulting in light hydrocarbons production. On the other hand, CO conversion was increased when the chain growth probability decreased (Bachara *et al*., 2001)

The comparison of the results obtained at different temperatures showed that the activity of all the catalysts were decreased when the temperature was decreased. However, the activity of bimodal mesoporous silica catalysts was higher than that of the monomodal mesoporous silica catalysts, in this case Co/BMS-1 catalyst presented the highest CO conversion. As the hydrocarbon product distribution of those catalysts was changed with FTS temperature, the product distribution was discussed in detail in the next section (Product Selectivity).

2.2 Product Selectivity

Significant differences can be observed in the FTS product distribution over the bimodal mesoporous silica catalysts that consisted of small and large pore sizes with different morphologies (Co/BMS-1, Co/BMS-2, and Co/BMS-3) and monomodal mesoporous silica catalysts (Co/SBA-3 and Co/SBA-15). The selectivity of Co/BMS-X catalysts during the FT synthesis are strongly affected by their pore structures and the structural properties of metallic cobalts. The different catalytic behaviors for each Co catalyst are reported as follows:

Concerning the cobalt supported monomodal mesoporous silica catalysts prepared by incipient wetness impregnation methods, it can be seen that Co/SBA-3 catalyst with 5 wt.% Co loading presented a high selectivity towards light hydrocarbon products (40%) and low selectivity towards heavy hydrocarbon products (C_5+) (approximately 60%), as shown in Table 6. The selectivity towards methane over Co/SBA-3 catalyst, which was undesired product, was significantly high (30%). In the case of bimodal mesoporous silica catalysts, the lower methane selectivity than monomodal mesoporous silica catalyst was observed. This could be attributed to the different pore structures of those catalysts as mentioned above. It was found that the

Co/BMS-1 catalyst gave the lowest selectivity towards methane (12.7 %) among all the catalysts.

The present investigation indicated that the product distribution was strongly affected by the pore structure and particle size of cobalt species. Comparing to Co/SBA-15 catalyst, the Co/SBA-3 catalyst with the smaller size of cobalt particles (as shown in Table 6 and Figure 28(a)) clearly exhibited higher selectivity to light hydrocarbons. The higher methane selectivity was in fact reported for catalysts having high metal dispersion, small Co metal size, and low Co reducibility (Sun *et al*., 2000). Khodakov *et al.,* (2002) found an inverse relationship between the methane selectivity and the overall extent of reduction for cobalt-supported mesoporous silica. The higher methanation activity of Co/SBA-3 could possibly lead to its low C_{5+} selectivity. It was noticed that the presence of larger cobalt particles could in contrast lead to higher selectivity to heavy hydrocarbons (Reuel *et al*., 1980). The selectivity towards C_5+ products was decreased from 70 % for Co/SBA-15 catalyst to 60 % for Co/SBA-3 catalyst.

In the case of BMS-X series of catalysts, since the catalytic properties of cobalt catalysts supported on silica were affected by the porosity and structure of supports. Therefore, the regular mesoporous structure of SBA-15 could possible promote mass transfer of reactants and products through the catalyst bed. This similar evidence was also found with Co/BMS-1 catalyst. The results revealed that Co/BMS-1 with the pore sizes of 6.5 and 3.8 nm displayed the highest C_{5+} selectivity and lowest methane selectivity as its large pore in bimodal mesoporous silica support could improve the product selectivity obtained from the catalyst with only small pore. Figure 29 clearly shows that the hydrocarbon product distribution of Co/BMS-X catalyst was shifted towards the formation of heavy hydrocarbons, especially C_{10}+ hydrocarbons, compared with the Co/SBA-3 and Co/SBA-15 catalysts. The Co/BMS-1 catalyst with two size, of cobalt particle size influence on the FTS product selectivity.

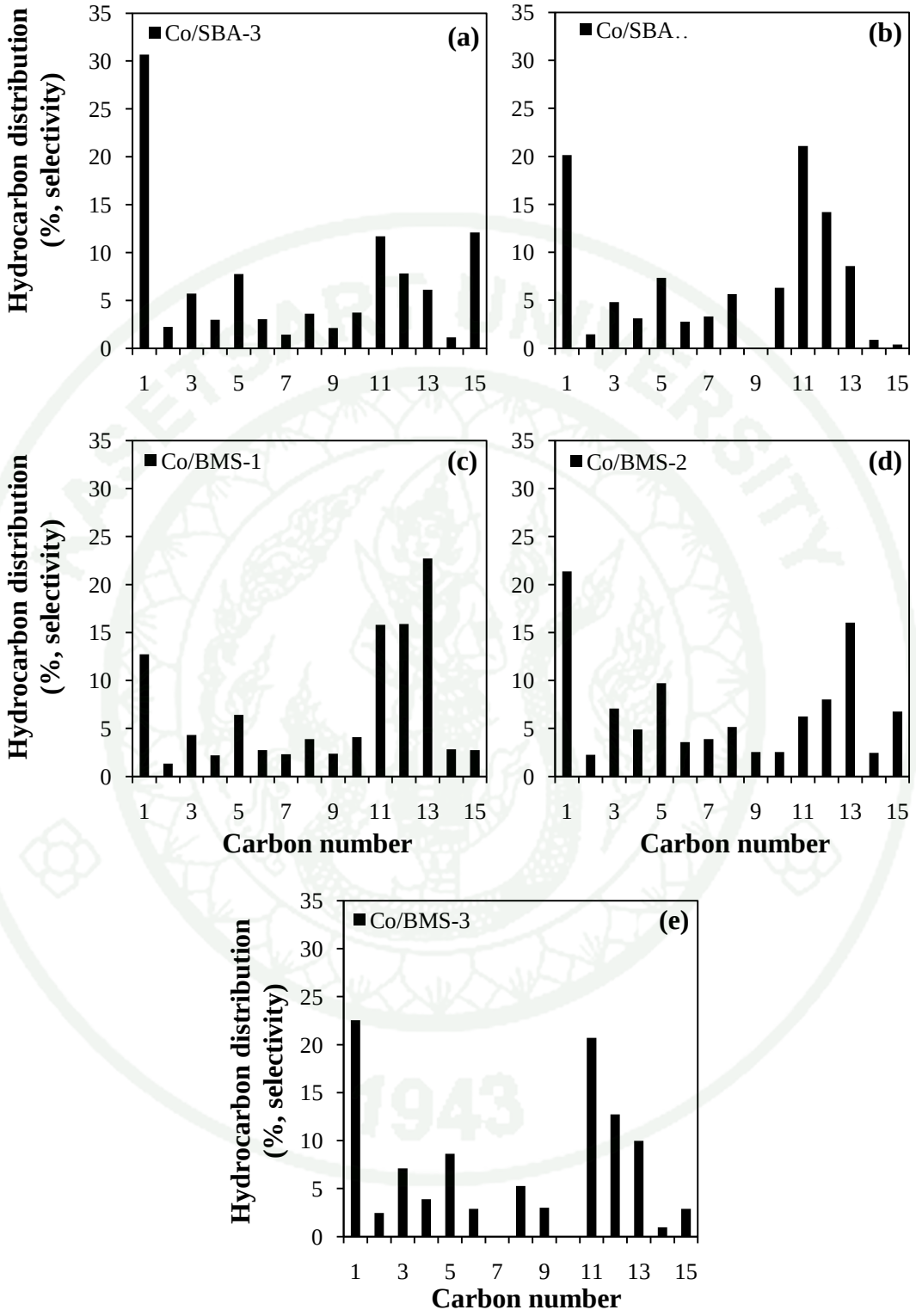

Figure 29 Hydrocarbon distributions (based on carbon atom) for (a) Co/SBA-3, (b) Co/SBA-15, (c) Co/BMS-1, (d) Co/BMS-2 and (e) Co/BMS-3 catalysts at 220 ºC (cobalt loading: 5 wt.%).

In the case of Co/BMS-2 catalyst, the thoroughly mixed phase between SBA-3 and SBA-15 were observed and displayed almost of Co particles dispersed in larger pores of SBA-15 and some of smaller Co particles dispersed in smaller pores of SBA-3. This phenomenon could be due to the cobalt nitrate solution hardly to diffuse into small pore of SBA-3 that infiltrated in SBA-15 mesoporous silica. As a result, the Co dispersion in Co/BMS-2 catalyst was similar to that of the Co/SBA-15 catalyst. As shown in Figure 29, the hydrocarbon distribution of Co/BMS-2 catalyst was therefore similar to that of Co/SBA-15 catalyst due to their similar Co dispersion on large pores of SBA-15.

Considering the pore structure of Co/SBA-3 catalyst, the pore blocking from cobalt aggregates were clearly observed. Therefore, the larger pore-size Co/SBA-15 catalyst, compared to Co/SBA-3 catalyst, could overcome the mass transfer limitation of reactants and hydrocarbon products (Khodakov *et al*., 2001) during the reaction was performed. As a result, the Co/SBA-15 catalyst with relatively larger pore size could enhance the diffusion of syngas and hydrocarbon products in mesoporous chanels, and the long chain hydrocarbons were selectivities produced. In the case of Co/BMS-1 catalyst, the higher C_{5+} selectivity and lower methane selectivity were obtained when compared to monomodal mesoporous catalysts. It was probably because of its large pore in bimodal mesoporous silica support of which could promote the formation of larger cobalt metal, leading to the formation of Co^0 which leads to higher selectivity to heavier hydrocarbon (Reuel and Bartholomew, 1984). As a result, the product selectivity towards higher hydrocarbons were found.

According to these result shown in Figures 29, 30 and 31, it can be clearly seen that the FTS product selectivity of cobalt supported catalyst depend on the reaction temperature. When the reaction temperature was decreased from 220 ºC to 180 ºC, the methane and C_2-C_4 selectivities (light hydrocarbons) was significant decreased, whereas C_{5+} selectivity was increased. It was due to the enthalpy of reaction of light hydrocarbons of which lower than those of heavy hydrocarbons (C_{5+}) (as shown in Table 7). When the reaction temperature was increased, methane and

C_2-C_4 selectivities were increased, this was due to the fact that the FTS reaction was strongly exothermic, as a result, the hydrocarbon products having lower enthalpies of reaction were then easily obtained. In the case of monomodal mesoporous silica catalyst, Co/SBA-15 with large pore diameters revealed the influence of the temperature on methane selectivity and C_{5+} selectivity. The methane selectivity was decreased from 20.1 % to 9.6 % and C_{5+} selectivity was increased from 70.5 % to 85.2 % when the reaction temperature was decreased for 40 ºC. In the case of Co/SBA-3 catalyst, methane selectivity was highest at all reaction temperatures. The result implied that the reaction temperature had the greater effect on the FTS product selectivity especially on Co/SBA-15 with larger pore diameter than Co/SBA-3 catalyst with smaller pore diameter.

Table 8 Enthalpies of formation of C_1-C_{10} alkanes

Reactions	$\Delta H°_{298}$* (kJ/mol)
$CO(g)+3H_2(g) \longrightarrow CH_4(g)+H_2O(g)$	-206
$2CO(g)+5H_2(g) \longrightarrow C_2H_6(g)+2H_2O(g)$	-347
$3CO(g)+7H_2(g) \longrightarrow C_3H_8(g)+3H_2O(g)$	-498
$4CO(g)+9H_2(g) \longrightarrow C_4H_{10}(g)+4H_2O(g)$	-672
$5CO(g)+11H_2(g) \longrightarrow C_5H_{12}(g)+5H_2O(g)$	-803
$6CO(g)+13H_2(g) \longrightarrow C_6H_{14}(g)+6H_2O(g)$	-955
$7CO(g)+15H_2(g) \longrightarrow C_7H_{16}(g)+7H_2O(g)$	-1,106
$8CO(g)+17H_2(g) \longrightarrow C_8H_{18}(g)+8H_2O(g)$	-1,259
$9CO(g)+19H_2(g) \longrightarrow C_9H_{20}(l)+9H_2O(g)$	-1,411
$10CO(g)+21H_2(g) \longrightarrow C_{10}H_{22}(l)+10H_2O(g)$	-1,562

$\Delta H°_{298}$ is calculated as: $\Delta H°_r$ = [$\sum \Delta H°_f$ products] - [*$\sum \Delta H°_f$ reactants].

In the case of bimodal mesoporous silica catalyst, Co/BMS-1 showed the lowest methane selectivity of 6.2 % at and highest C_{5+} selectivity of 89.6 % at 180 ºC. Similar trends were obtained from Co/BMS-2 and Co/BMS-3 catalysts, when the reaction temperature was decreased, the lower methane and higher C_{5+} selectivity were obtained (as shown in table 7). As a result, the product selectivity towards higher hydrocarbons (C_{5+}) was obtained when the reaction temperature was decreased. This was because at higher reaction temperatures would cause an increase in hydrogenation activity and production of light hydrocarbons (Bechara *et al*., 2001), whereas olefins were preferentially hydrogenated and chain propagation was suppressed (Sharifnia *et al*., 2005).

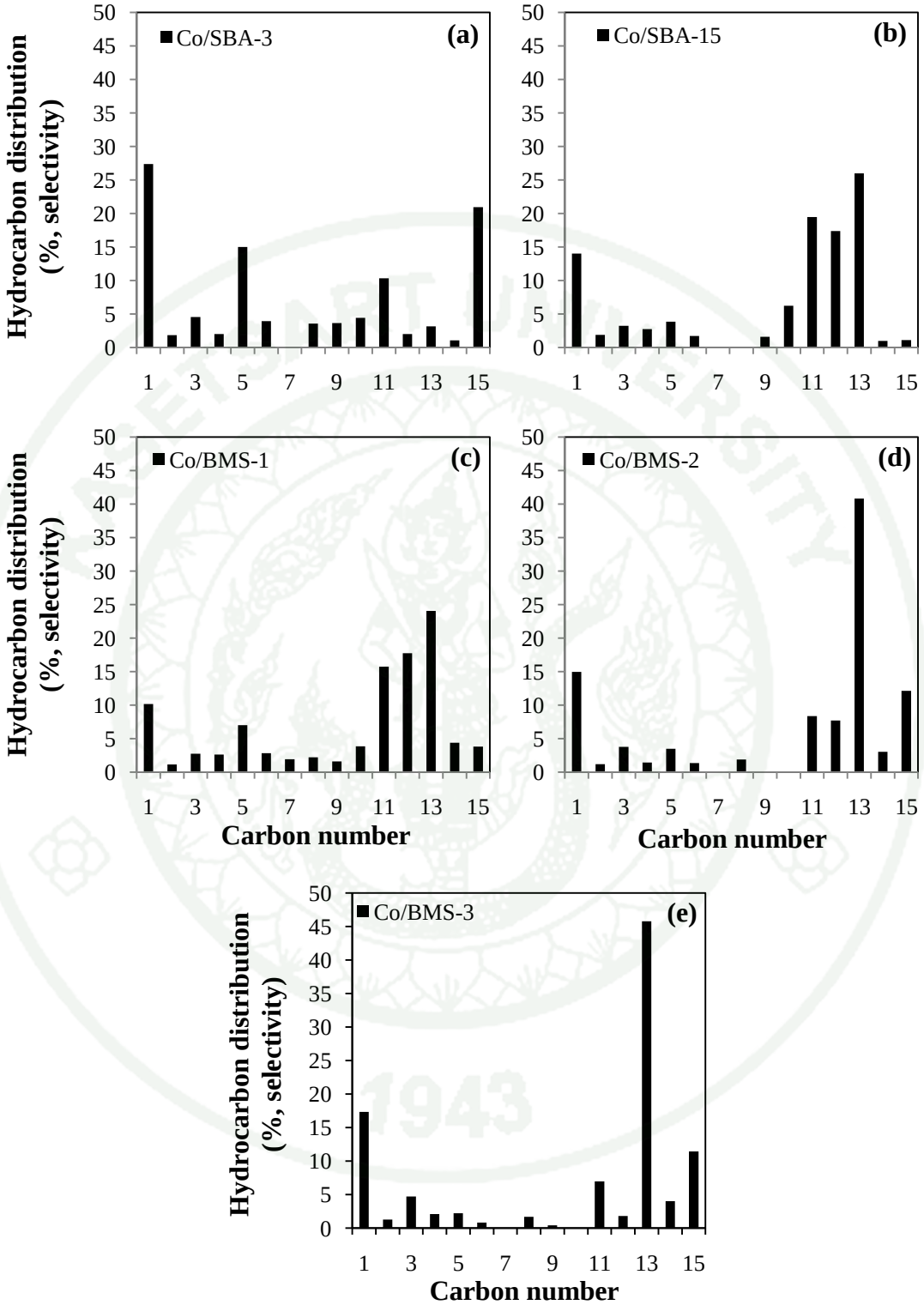

Figure 30 Hydrocarbon distributions (based on carbon atom) for (a) Co/SBA-3, (b) Co/SBA-15, (c) Co/BMS-1, (d) Co/BMS-2 and (e) Co/BMS-3 catalysts at 200 ºC (cobalt loading: 5 wt.%).

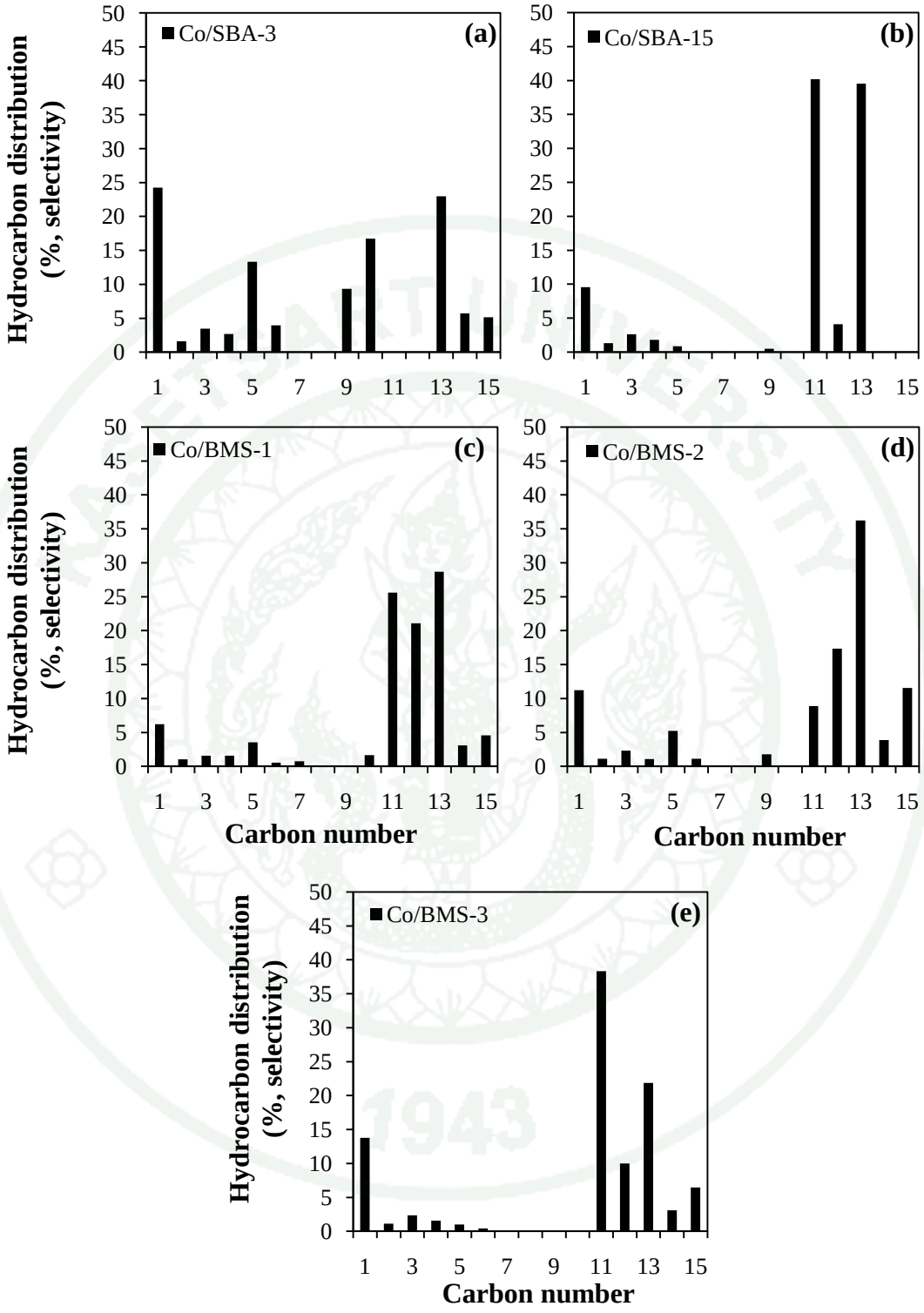

Figure 31 Hydrocarbon distributions (based on carbon atom) for (a) Co/SBA-3, (b) Co/SBA-15, (c) Co/BMS-1, (d) Co/BMS-2 and (e) Co/BMS-3 catalysts at 180 ºC (cobalt loading: 5 wt.%).

It can be concluded that bimodal mesoporous silica catalysts could be potentially applied to prepare the FTS catalyst. In the case of monomodal mesoporous silica catalyst. The undesired methane product, normally occurred over monomodal mesoporous silica with small pore diameter and high cobalt dispersion, was distinguishly reduced while the long-chain hydrocarbon products, particularly the gasoline-range, were remarkably promoted over the Co/SBA-15 catalyst. The selectivities of gasoline and naphtha products were relatively increased from 41.2 % and 29.0 % to 60.6 % and 47.2 %, respectively. When compared between Co/SBA-3 and Co/SBA-15 catalysts. (as shown in Figure 32(a)). In the case of bimodal mesoporous silica catalysts, especially Co/BMS-1 the lowest selectivity of methane and highest selectivity of diesel product when compared to monomodal mesoporous silica catalysts were observed (as shown in Figure 32(b)).

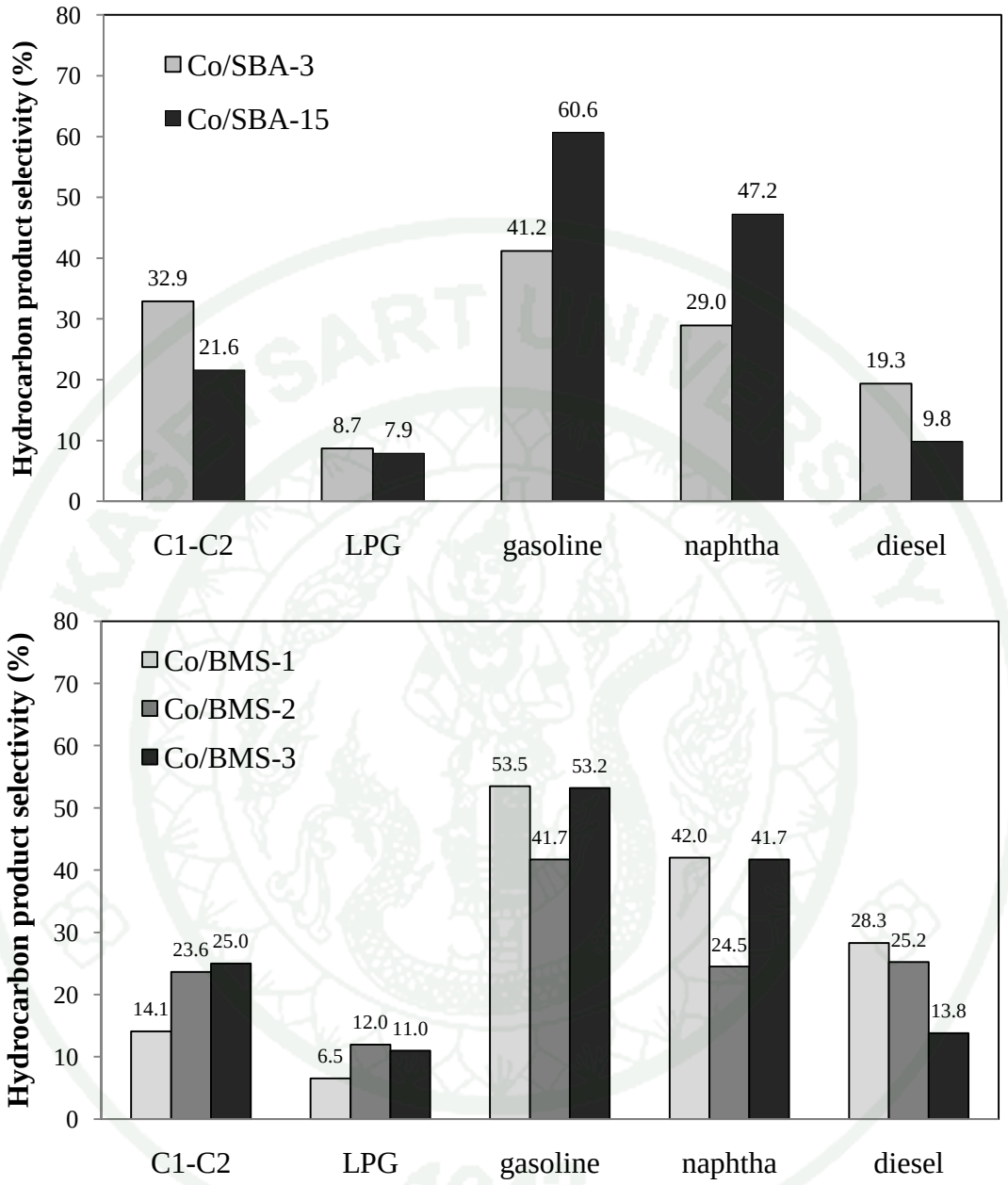

Figure 32 Variation of FTS products including fuel gas (C_1-C_2), LPG (C_3-C_4), gasoline (C_4-C_{12}), naphtha (C_8-C_{12}) and diesel (C_{12}-C_{15}) over 5 %.wt cobalt loaded on (a) Co/SBA-3 and Co/SBA-15 catalyst (b) bimodal mesoporous silica catalysts including Co/BMS-1, Co/BMS-2 and Co/BMS-3 catalysts.

CONCLUSION

The cobalt supported bimodal mesoporous silica catalysts were prepared by the incipient wetness impregnation method using cobalt nitrate as a cobalt precursor. The obtained catalysts were tested for Fisher-Tropsch synthesis performance and compared to those of monomodal mesoporous silica catalysts. The result can be concluded as follows:

1. The support porosity had strongly influenced both on the size of cobalt catalysts over porous silica supports and also on the FTS performance. The Co_3O_4 crystallite size was increased with increasing the mesopore size of porous silica supports, and two size of cobalt particle occurred in different pore size diameters in bimodal porous silica catalysts.

2. It was found that Co/BMS-1 catalyst was much more active (14.1 % CO conversion) than monomodal mesoporous silica catalyst including Co/SBA-15 and Co/SBA-3 at the similar cobalt loading amount. The higher FTS activity of the BMS-X catalyst was attributed to the mixed-phase structural morphologies of SBA-3 and SBA-15 in these catalysts.

3. The FTS product selectivity towards methane over Co/BMS-1 catalyst was low (12.7 %) while the selectivity towards heavy hydrocarbon product (C_{5+}) was relatively high (81.7 %) compared to other catalysts.

LITERATURE CITED

Afonso, J.C., D. A.G. Aranda, M. Schmal and R. Frety. 1997. Regeneration of a Pt/Al_2O_3 catalyst: influence of heating rate, temperature and time of regeneration. **Fuel Proc. Tech.** 50: 35-48.

Aguado, J., G. Calleja, A. Carrero and J. Moreno. 2008. One-step synthesis of chromium and aluminium containingSBA-15 materials: New phillips catalysts for ethylene polymerization. **J. Chem. Eng.** 137: 443–452.

Bagshaw, S.A., E. Prouzet and T.J. Pinnavaia. 1995. Templating of Mesoporous Molecular Sieves by Nonionic Polyethylene Oxide Surfactants. **Science.** 269: 1242-1244.

Bechara, R., D. Balloy and D. Vanhove. 2001. Catalytic properties of Co/Al_2O_3 system for hydrocarbon synthesis. **Appl. Catal. A: General.** 207: 343-353.

Beck, J.S., J.C. Vartuli, W.J. Roth, M.E. Leonowicz, C.T. Kresge, K. D. Schmitt, C. T-W. Chu, D. H. Olson, E.W. Sheppard, S.B. McCullen, J.B. Higgins and J.L. Schlenkert. 1992. A new family of mesoporous molecular sieves prepared with liquid crystal templates. **J. Am. Chem. Soc**. 114: 10834-10843.

Bertole, C.J., C.A. Mims and G. Kiss. 2004. Support and rhenium effects on the intrinsic site activity and methane selectivity of cobalt Fischer–Tropsch catalysts. **J. Catal**. 221: 191–203.

Bharat, L., N.J. Olanrewaju and S. Komarneni. 2001. Direct synthesis of titanium-substituted mesoporous SBA-15 molecular sieve under microwave-hydrothermal conditions. **Chem. Mater**. 13: 552-557.

Bhoware, S.S. and A.P. Singh. 2006. Characterization and catalytic activity of cobalt containing MCM-41 prepared by direct hydrothermal, grafting and immobilization methods. **J. Mol. Catal. A: Chem**. 266: 118-130.

Bian, G., N. Fujishita, T. Mochizuki, W. Ning, M. Yamada. 2003. Investigations on the structural changes of two Co/SiO_2 catalysts by performing Fischer–Tropsch synthesis. **Appl. Catal. A:** 252: 251-260.

Cai, Q., Z.S. Lue, W.Q. Pang, Y.W. Fan, X.H. Chen and F.Z. Cui. 2001. Dilute solution Routes to various controllable morphologies of MCM-41 silica with a basic medium. **Chem. Mater**. 13: 258-263.

Chanenchuk, C.A., I.C. Yates and C.N. Satterfield. 1991. The Fischer-Tropsch synthesis with a mechanical mixture of a cobalt catalyst and a copper-based water gas shift catalyst. **Energy and Fuels** 5: 847-855.

Chareonpanich, M., T. Namto, P. Kongkachuichay and J. Limtrakul. 2004. Synthesis of ZSM-5 zeolite from lignite fly ash and rice husk ash. **Fuel Proc. Tech.** 85: 1623-1634.

_____, A. Nanta-ngern and J. Limtrakul. 2007. Short-period synthesis of ordered mesoporous silica SBA-15 using ultrasonic technique. **Mater. Lett**. 61: 5153–5156.

_____, O. Jullaphan and T. Witoon. 2009. Synthesis of mixed-phase uniformly infiltrated SBA-3-like in SBA-15 bimodal mesoporous silica from rice husk ash. **Mater. Lett**. 63: 1303-1306.

Chen, C.Y., S.L. Burkett, H.X. Li and M.E. Davis. 1993. Studies on mesoporous materials II. Synthesis mechanism of MCM-41. **Micropor. and Mesopor. Mater**. 2: 27-34.

Chin, R.L. and D.M. Hercules. 1982. Surface spectroscopic characterization of cobalt-alumina catalysts. **J. Phy. Chem.** 86: 360-367.

Coma, A. 1997. From microporous to mesoporous molecular sieve materials and their use in catalysis. **Chem. Rev**. 97: 2373-2379

Coppens, M.O., J. Sun and T.Maschmeyer. 2001. Synthesis of hierarchical porous silicas with a controlled pore size distribution at various length scales. **Catal. Today**. 69: 331–335.

Coulter, K. E. and A. G. Sault. 1995. Effects of activation on the surface properties of silica-supported cobalt catalysts**. J. Catal**. 154: 56-64.

Dalai, A.K. and B.H. Davis. 2008. Fischer–Tropsch synthesis: A review of water effects on the performances of unsupported and supported Co catalysts. **Appl. Catal. A: General**. 348: 1-15

Davis, B.H. 2001. Fischer-Tropsch synthesis: current mechanism and futuristic needs**. Fuel Proc. Tech.** 71:157-166.

Das, T.K., G. Jacobs, P.M. Patterson, W.A. Conner, J. Li and B.H. Davis. 2003. Fischer–Tropsch synthesis: characterization and catalytic properties of rhenium promoted cobalt alumina catalysts. **Fuel Proc. Tech.** 82: 805– 815.

Dry, M.E. 1990. The fischer-tropsch process - commercial aspects. **Catal. Today.** 6: 183-206.

_____. 1996. Practical and theoretical aspects of the catalytic Fischer-Tropsch process. **Appl. Catal. A: General**. 138 (2): 319-344.

_____. 2002. The Fischer–Tropsch process: 1950–2000. **Catal. Today.** 71: 227–241.

Dunn, B.C., G.C. Turpin, P. Cole, M.C. Webster, Z. Ma, R.J. Pugmire, R.D. Earnst and E.M. Eyring. 2004. Cobalt and ruthenium Fischer-Tropsch catalysts supported on silica aerogel. **Am. Chem. Soc., Divis. Petro. Chem.** 49: 431-434.

Ernst, B., S. Libs, P. Chaumette, A. Kiennemann. 1999. Preparation and characterization of Fischer-Tropsch active Co/SiO2 catalysts. **Appl. Catal. A: General**. 186: 145–168.

Fan, J., C.Z. Yu and T. Gao. 2003. Cubic mesoporous silica with large controllable entrance sizes and advanced adsorption properties. **Angew. Chem. Int. Ed**. 42(27):3146-3150.

Fan, J., and J. Lei. 2005. Low-temperature strategy to synthesize highly ordered mesoporous silicas with very large pores. **J. Am. Chem. Soc**. 127(31): 10794–10795.

Girardon, J.S., A.S. Lermontov, L. Gengembre, P.A. Chernavskii, A.G. Constanta and A.Y. Khodakov. 2005. Effect of cobalt precursor and pretreatment conditions on the structure and catalytic performance of cobalt silica-supported Fischer–Tropsch catalysts. **J. Catal**. 230: 339-352.

Grieken, R.V., J.M. Escola, J. Moreno and R. Rodriguez. 2006. Liquid phase oligomerization of 1-hexene over different mesoporous aluminosilicates (Al-MTS, Al-MCM-41 and Al-SBA-15) and micrometer/nanometer HZSM-5 zeolites. **Appl. Catal. A: General**. 305: 176-188.

Guari, Y., C. Thieuleux, A. Mehdi, C. Reye, R.J.P. Corriu, S. Gomez-Gallardo, K. Philippot, B. Chaudret and R. Dutartre. 2001. In-situ formation of gold nanoparticles within functionalized ordered mesoporous silica via an organometallic chimie douce approach. **Chem. Commun**. 1374-1375.

Hosseini, S.A., A. Taeb, F. Feyzi and F. Yaripour. 2004. Fischer-Tropsch synthesis over Ru promoted Co/γ-Al_2O_3 catalysts in a CSTR. **Catal. Commun**. 5: 137-143.

Hurlbut, R.S., I. Puskas and D.J. Schumacher. 1996. Fine details on the selectivity and kinetics of the Fischer–Tropsch synthesis over cobalt catalysts by combination of quantitative gas chromatography and modeling, **Energy Fuels.** 10: 537– 545.

Inagaki, S., Y. Fukushima and K. Kuroda. 1993. Synthesis of highly ordered mesoporous materials from a layered polysilicate. **J. Chem. Soc., Chem. Commun**. 1993: 680-682.

Iglesia, E., S. L. Soled and R. A. Fiato. 1992. Fischer-Tropsch synthesis on cobalt and ruthenium: Metal dispersion and support effects on reaction rate and selectivity. **J. Catal.** 137: 212-224.

_____, 1997. Design, synthesis, and use of cobalt-based Fischer-Tropsch synthesis catalysts. **Appl. Catal. A: General**. 161: 59-78.

Jacobs, G., T. K. Das, Y.Zhang, J. Li, G. Racoillet and B. H. Davis. 2002. Fischer-Tropsch synthesis: support, loading, and promoter effects on the reducibility of cobalt catalysts. **Appl. Catal. A: General**. 233: 263 -281.

Jalama, K., N.J. Coville, D. Hildebrandt, D. Glasser and L.L. Jewell. 2007. Fischer–Tropsch synthesis over Co/TiO_2: Effect of ethanol addition. **Energy Fuels** 86: 73-80.

Jana, S.K., T. Kugita and S. Namba. 2003. Bisphenol F synthesis over mesoporous aluminosilicate MCM-41 molecular sieves. **Catal. Lett**. 90: 143-147.

Khodakov, A.Y., A. Griboval-Constant, R. Bechara and V.L. Zholobenko. 2002. Pore size effects in Fischer-Tropsch synthesis over cobalt-supported mesoporous silicas. **J. Catal.** 206: 230-241.

_____, R. Bechara and A. Griboval-Constant. 2003. Fischer-Tropsch synthesis over silica supported cobalt catalysts: mesoporous structure versus cobalt surface density. **Appl. Catal. A: General.** 254: 273-288.

_____. 2005. Effect of cobalt precursor and pretreatment conditions on the structure and catalytic performance of cobalt silica-supported Fischer–Tropsch catalysts. **J. Catal.** 230: 339-352.

Kleitz, F., S.H. Choi and R. Ryoo. 2003. Cubic Ia3d large mesoporous silica: synthesis and replication to platinum nanowires, carbon nanorods and carbon nanotubes. **Chem. Commun.** 17: 2136–2137.

Knottenbelt, C. 2002. Mossgas "gas-to-liquid" diesel fuels—an environmentally friendly option. **Catal. Today.** 71: 437–445.

Kodama, T., T. Shimizu, K. Shimizu and Y. Kitayama. 2001. Thermochemical methane reforming using WO_3 as an oxidant below 1173 K by a solar furnace simulator. **Solar Energy**. 71(5): 315-324.

Konya, Z., V.F. Puntes, I. Kiricsi, J. Zhu, P. Alivisatos and G.A. Somorjai. 2002. Novel Two-Step Synthesis of Controlled Size and Shape Platinum nanoparticles Encapsulated in Mesoporous Silica. **Catal. Lett**. 81: 137-140.

Kresge, C.T., A.W. Chester and S.M. Oleck. 1992. Control of metal radial profiles in alumina supports by carbon dioxide. **Appl. Catal. A: General**. 81(2): 215-226.

Kruk, M. and M. Jaroniec. 2000. Characterization of the porous structure of SBA-15. **Chem. Mater.** 12: 1961-1968.

Li, H., S. Wang, F. Ling and J. Lii. 2006. Studies on MCM-48 supported cobalt catalyst for Fisher-Tropsch synthesis. **J. Catal**. **A**. 244: 33–40.

Li, Y., Z. Feng, Y. Lian, K. Sun, L. Zhang, G. Jia, Q. Yang and C. Li. 2005. Direct synthesis of highly ordered Fe-SBA-15 mesoporous materials under weak acidic conditions. **Micropor. Mesopor. Mater**. 84: 41–49.

Liu, Y., Y. Zhang, G. Yang, S. Sun and N. Tsubaki. 2007. Effects of impregnation solvent on Co/SiO_2 catalyst for Fischer-Tropsch synthesis: A highly active and stable catalyst with bimodal sized cobalt particles. **Appl. Catal. A: General**. 321: 79-85.

Loosdrecht J.V., M.V. Haar, A. M. Kraan, A. J. Dillen and J. W. Geus. 1997. Preparation and properties of supported cobalt catalysts for Fischer-Tropsch synthesis. **Appl. Catal. A: General**. 150: 365-376.

Luo, M. and B.H. Davis. 2003. Fischer–Tropsch synthesis: activation of low-alpha potassium promoted iron catalysts. **Fuel Proc. Tech.** 83 (1-3): 49-65.

Lou, Z., R. Wang, H. Sun, Y. Chen and Y. Yang. 2008. Direct synthesis of highly ordered Co-SBA-15 mesoporous materials by the pH-adjusting approach. **Micropor. and Mesopor. Mater**. 110: 347-354.

Martínez, A., C. Lopez, F. Marquez and I. Diaz. 2003. Fischer–Tropsch synthesis of hydrocarbons over mesoporous Co/SBA-15 catalysts: the influence of metal loading, cobalt precursor, and promoters. **J. Catal**. 220: 486–499.

Melero, J. A., J. M. Arsuaga, P.D. Frutos, J. Iglesias, J. Sainz and S. Blazquez. 2005. Direct synthesis of titanium-substituted mesostructured materials using non-ionic surfactants and titanocene dichloride. **Micropor. and Mesopor. Mater.** 86: 364-373.

Ming, H. and B.G. Baker. 1995. Characterization of cobalt Fischer-Tropsch catalysts of unpromoted cobalt-silica gel catalysts. **Appl. Catal. A: General**. 123: 23-36.

Mirji, S.A., S.B. Halligudi, N. Mathew, N.E. Jacob, K.R. Patil and A.B. Gaikwad. 2007. Adsorption of methanol on mesoporous SBA-15. **Mater. Lett.** 61: 88-92.

Mochizuki, T., T. Hara, N. Koizumi and M.Yamada. 2006. Surface structure and Fischer–Tropsch synthesis activity of highly active Co/SiO_2 catalysts prepared from the impregnating solution modified with some chelating agents. **Appl. Catal. A: General**. 317: 97–104.

Nanta-Ngern, A. 2005. **The Synthesis of SBA-15 Mesoporous Silica from Rice Husk Ash.** M.S. Thesis, Kasetsart University.

Ohtsuka, Y., Y. Takahashi, M. Nogushi, T. Arai, S. Takasaki, N. Tsubouchi and Y. Wang. 2004. Novel utilization of mesoporous molecular sieves as supports of cobalt catalysts in Fischer-Tropsh synthesis. **Catal. Today**. 89: 419-429.

Prashar, A.K., R.P. Hodgkins, R. Kumar and R.N. Devi. 2008. In situ synthesis of Pt nanoparticles in SBA-15 by encapsulating in modified template micelles: sized restricted growth within the mesochannels. **J. Mater**. **Chem.** 18: 1765–1770.

Prieto, G., A. Martınez, R. Murciano and M.A. Arribas. 2009. Cobalt supported on morphologically tailored SBA-15 mesostructures: The impact of pore length on metal dispersion and catalytic activity in the Fischer–Tropsch synthesis. **Appl. Catal. A.** 367: 146-156.

Reubroycharoen, P., T. Vitidsant, Y. Lui, G. Yang and N. Tsubaki. 2007. Highly active Fischer-Tropsch synthesis Co/SiO2 catalysts prepared from microwave irradiation. **Catal. Commun**. 8: 375-378.

Reuel, R.C. and C.H. Bartholomew. 1984. The stoichiometries of H_2 and CO adsorptions on cobalt: Effects of support and preparation. **J. Catal**. 85: 63-77.

Rohr, F., O.A. Lindvag, A. Holmen and E.A. Blekkan. 2000. Fischer–Tropsch synthesis over cobalt catalysts supported on zirconia-modified alumina, **Catal. Today.** 58: 247– 254.

Saib, A.M., M. Claeys and E.V. Steen. 2002. Silica supported cobalt Fischer-Tropsch catalysts: effect of pore diameter of support. **Catal. Today.** 71: 395-402.

Schulz, H. 1999. Short history and present trends of Fisher-Tropsch synthesis. **Catal. A: General**. 186: 3-12.

_____ and M. Claeys. 1999. Reactions of a-olefins of different chain length added during Fischer–Tropsch synthesis on a cobalt catalyst in a slurry reactor. **Appl. Catal. A: General**. 186: 71–90.

Selvaraj, M., A. Pandurangan, K.S. Seshadri, P.K. Sinha and K.B. Lal. 2002. Synthesis, characterization and catalytic application of MCM-41 mesoporous molecular sieves containing Zn and Al. **Appl. Catal. A: General**. 242: 347-364.

Selvaraj, M and S. Kawi. 2008. Direct synthesis and catalytic performance of ultralarge pore GaSBA-15 mesoporous molecular sieves with high gallium content. **Catal. Today.** 131: 82-89.

Shah, P., A.V. Ramaswamy, K. Lazar and V. Ramaswamy. 2007. Direct hydrothermal synthesis of mesoporous Sn-SBA-15 materials under weak acidic conditions. **Micropor. and Mesopor. Mater.** 100: 210-226.

Sharifnia, S., Y. Mortazavi and A. Khodadadi. 2005. Enhancement of distillate selectivity in Fischer–Tropsch synthesis on a Co/SiO_2 catalyst by hydrogen distribution along a fixed-bed reactor. **Fuel Proc. Tech**. 86(12-13): 1253-1264.

Shinoda, M., Y. Zhang, Y. Yoneyama, K. Hasegawa and N. Tsubaki. 2004. New bimodal pore catalysts for Fischer–Tropsch synthesis. **Fuel Proc. Tech.** 86: 73– 85.

Siriluk, C. and S. Yuttapong. 2005. **8th Asian Symposium on Visualization**. Chiangmai, Thailand.

Song, D. and J. Li. 2006 Effect of catalyst pore size on the catalytic performance of silica supported cobalt Fischer-Tropsch catalysts. **J. Mol. Catal. A: Chem.** 247: 206- 212.

Steen, E.V., G.S. Sewell, R.A. Makhothe, C. Micklethwaite, H. Manstein, M. Lange and C.T. O'Connor. 1996. TPR Study on the Preparation of Impregnated Co/SiO_2 Catalysts. **J. Catal**. 162: 220-229.

Sun, J.H., Z. Shan, T. Maschmeyer and M.O. Coppens. 2003. Synthesis of Bimodal Nanostructured Silicas with Independently Controlled Small and Large Mesopore Sizes. **Langmuir**. 19: 8395-8402.

Sun, S., N. Tsubaki and K. Fujimoto. 2000. The reaction performances and characterization of Fischer-Tropsch synthesis Co/SiO_2 catalysts prepared from mixed cobalt salts. **Appl. Catal. A: General**. 202: 121-131.

Takahashi, R., S. Sato, T. Sodesawa, T. Goto, K. Matsutani and N. Mikami. 2007. Bending strength of silica gel with bimodal pores: Effect of variation in mesopore structure. **Mater. Res. Bull.** 40: 1148–1156.

Takeshita, T. and K. Yamaji. 2008. Important roles of Fischer-Tropsch synfuels in the global energy future. **Energy Policy**. 36: 2773– 2784.

Tanev, P.T., M. Chibwe and T.J. Pinnavaia. 1994. Titanium-containing mesoporous molecular sieves for catalytic oxidation of aromatic compounds. **Nature.** 368 321-323.

Tavasoli, A., M.G. Ahangari, C. Soni, A.K. Dalai. 2008. Cobalt supported on carbon nanotubes-Apromising novel Fischer-Tropsch synthesis catalyst. **Fuel Proc. Tech.** 89: 491-498.

Tavasoli, A., K. Sadaghiani, A. Nakhaeipour and M. Ahangari. 2007. Cobalt loading effects on the structure and activity for Fisher-Tropsch and water-gas shift reactions of Co/Al_2O_3. **J. Chem. Eng**. 26(1): 1-5.

Tsubaki, N., Y. Zhang, S. Sun, H. Mori, Y. Yoneyama, X. Li, K. Fujimoto. 2001. A new method of bimodal support preparation and its application in Fischer-Tropsch synthesis. **Catal. Commun.** 2: 311.

Tuel, A., V. Gramlich, Ch. Baerlocher. 2004. Synthesis and crystal structure of a new layered aluminophosphate $[Al_3P_4O_{16}][C_6N_3H_{17}][H_3O]$. **J. Solid State Chem**. 177: 2484-2493.

Van Der Laan, G.P. and A. A. C. M. Beenackers. 1999. Kinetics and Selectivity of the Fischer-Tropsch Synthesis: A Literature Review. **Catal. Rev.** 41: 255–318.

Vannice, M.A. 1977. The catalytic synthesis of hydrocarbons from H_2/CO mixtures over the Group VIII metals V. The catalytic behavior of silica-supported metals. **J. Catal.** 50: 228-236.

Vinu, A., P. Srinivasu, C. Anand, S.Alam, K. Ariga, S. B. Halligudi and V. V. Balasubramanian . 2008. Direct synthesis and the morphological control of highly ordered two-dimentional P6mm mesoporous nionium silicates with high niobium content. **J. Phy. Chem.** 112: 10130-10140.

Wan, Y. and D. Zhao. 2007. On the Controllable Soft-Templating Approach to Mesoporous Silicates. **Chem. rev.** 107(7): 2821-2860.

Wang, L., A. Kong, B. Chen, H. Ding, Y. Shan and M. He. 2005. Direct synthesis, characterization of Cu-SBA-15 and its high catalytic activity in hydroxylation of Phenol by H2O2. **J. Mol. Catal. A: Chem.** 230: 143-150.

Xiong, H., Y. Zhang, K. Liew and Jinlin Li. 2008. Fischer–Tropsch synthesis: The role of pore size for Co/SBA-15 catalysts. **J. Mol. Catal. A: Chem.** 295: 68-76.

Yang, Y., Y. Liu, G. Yang, S. Sun and N. Tsubaki. 2007. Effect of impregnation solvent on Co/SiO2 catalyst for Fischer-Tropsch synthesis: A highly active and stable catalyst with bimodal sized cobalt particles. **Appl. Catal. A: General**. 79-85.

Zennaro, R., M. Tagliabue and C.H. Bartholomew. 2000. Kinetics of Fischer-Tropsch synthesis on titania-supported cobalt. **Catal. Today.** 58: 309-319.

Zhang, C.H., Y. Yang, B.T. Teng, T.Z. Li, H.Y. Zheng, H.W. Xiang and Y.W. Li. 2006. Study of an iron-manganese Fischer–Tropsch synthesis catalyst promoted with copper. **J. Catal**. 237: 405-415.

Zhang, Y., Y. Liu, G. Yang, S. Sun and N. Tsubaki. 2007. Effect of impregnation solvent on Co/SiO_2 catalyst for Fischer-Tropsh synthesis: A highly active and stable catalyst with bimodal sized cobalt particles. **Appl. Catal. A: General.** 321: 79-85.

Zhang, Y., X. Shi, J. M. Kim, D. Wu, Y. Suna and S. Peng. 2004. Synthesis and catalysis of nanometer-sized bimodal mesoporous aluminosilicate materials. **Catal. Today.** 93–95: 615–618.

Zhao, D., J. Feng, Q. Huo, N. Melosh, G.H. Fredrickson, B.F. Chmelka and G.D. Stucky. 1998. Triblock copolymer syntheses of mesoporous silica with periodic 50 to 300 angstrom pores. **Science** 279: 548-552.

Zholobenko, V.L., A. Evans, D. Plant and S.M. Holmes. 2001. Acid sites in mesoporous materials: a DRIFTS study. **Micropor. and Mesopor. Mater.** 44-45: 793-799.

APPENDICES

Appendix A

Qualitative and Quantitative Results from Gas Chromatography

Quantitative and Qualitative Results from Gas Chromatography

Gas chromatography was performed in a specially designed instrument. The major instrumental components consisted of a flowing mobile phase, an injector port, a separation column containing the stationary phase, a detector, and a data recording system as shown in Appendix Figure A1. Certain amount of gaseous mixture, 0.5 mL in this research, was injected into gas chromatograph at the injector port and was volatilized in a hot injection chamber before it was transported to the head of the chromatic column. Then, a flow of inert carrier gas (as a mobile phase) swept the injected mixture through a heated column which contained the stationary phase. The gaseous sample moved along the packing column whereas its component gas moved with different flow rates and thus separated into pure component. Before each component exited the instrument, it passed through a detector. The detector sent an electronic signal to the recorder and the analyzed results were printed out.

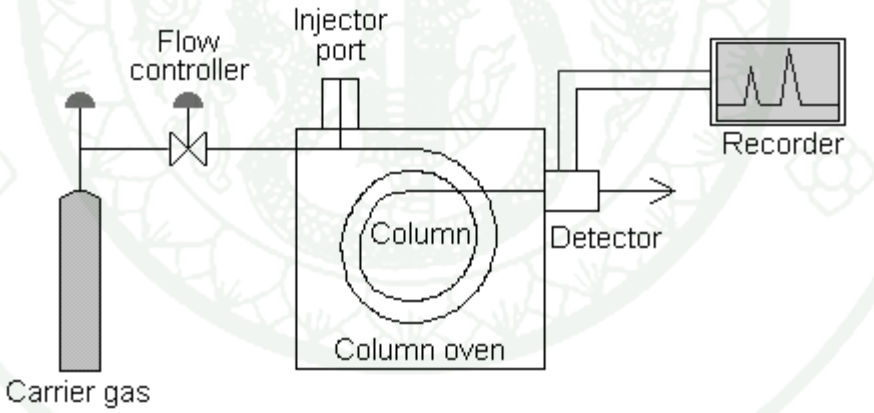

Appendix Figure A1 Schematic diagram of gas chromatograph.

In this work, the quantitative and qualitative data of product composition was obtained from 2 types of gas chromatography including TCD-GC and FID-GC as mention in the experimental chapter. Before analysis, the condition of operation was set and kept on running for about an hour to stabilize the based line. Certain volume of sample mixture (0.5 mL in this case) was injected into the injection port by gas syringe. After the mixture of sample gas was analyzed, the qualitative and

quantitative data were interpreted from the peak area obtained from the recorder. The component of injected gas mixture can be identified by using the value of retention time data compared with the retention time received from injected standard gas. The chromatogram of standard gases and liquids used in this research were shown as following figures:

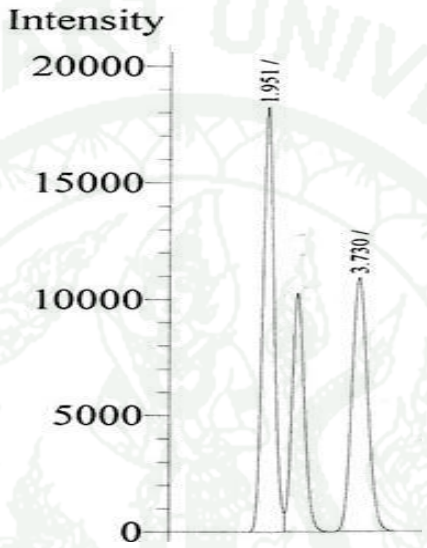

Appendix Figure A2 Chromatogram of standard gases for CO and CO_2.

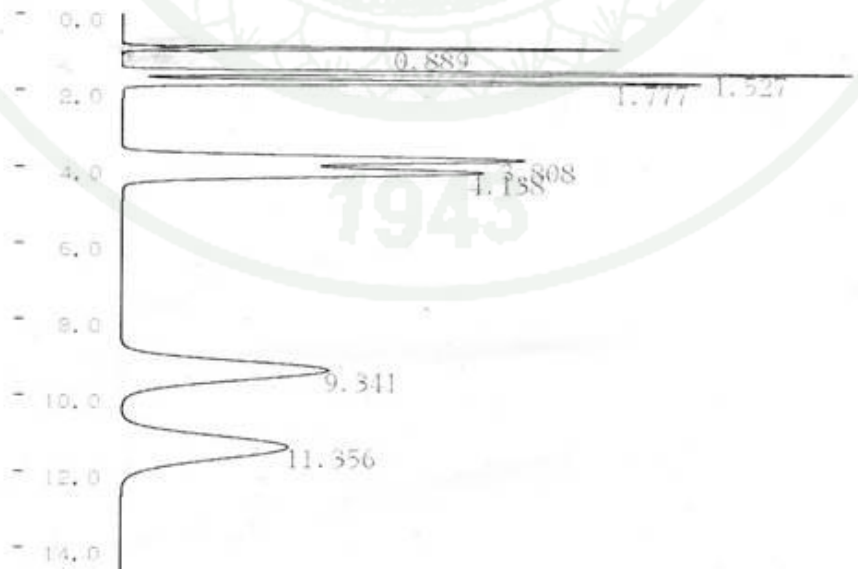

Appendix Figure A3 Chromatogram of standard gases for C_1-C_4 hydrocarbons.

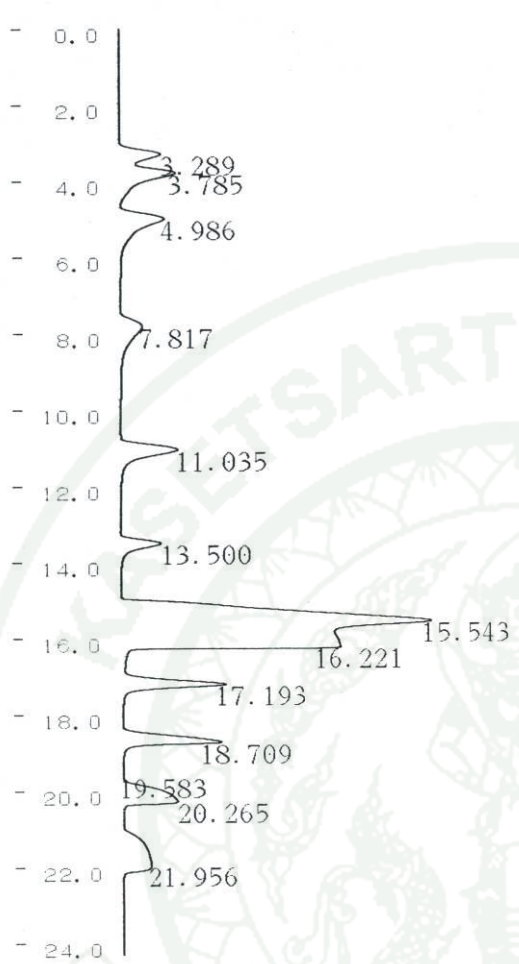

Appendix Figure A4 Chromatogram of standard liquids for C_5-C_{15} hydrocarbons.

The quantitative analysis of gas and liquid samples were obtained from the calibration curves where the correlation between the amount of injected gas or liquid sample (mole) and the peak area of gas chromatograms were proposed. The correlation between these parameters (mole and area) was analyzed by a linear regression equation. All the calibration curves for each single standard gas and liquid used in this research were shown in Appendix Table A1.

Appendix Table A1 Equation of calibration curves for standard gas and liquid

Substance	Equation	R^2
CO	mol = 4.46×10^{-11} x area	0.999
CO_2	mol = 4.38×10^{-11} x area	0.999
CH_4	mol = 1.11×10^{-12} x area	0.999
C_2H_4	mol = 4.55×10^{-13} x area	0.996
C_2H_6	mol = 5.22×10^{-13} x area	0.998
C_3H_6	mol = 3.65×10^{-13} x area	0.999
C_3H_8	mol = 3.68×10^{-13} x area	0.998
C_4H_{10}	mol = 2.79×10^{-13} x area	0.999
C_5H_{12}	mol = 3.05×10^{-13} x area	0.997
C_6H_{14}	mol = 1.39×10^{-13} x area	0.997
C_7H_{16}	mol = 1.39×10^{-13} x area	0.997
C_8H_{18}	mol = 1.97×10^{-13} x area	0.997
C_9H_{20}	mol = 1.13×10^{-13} x area	0.997
$C_{10}H_{22}$	mol = 1.97×10^{-13} x area	0.988
$C_{11}H_{24}$	mol = 7.36×10^{-14} x area	0.995
$C_{12}H_{26}$	mol = 6.85×10^{-14} x area	0.996
$C_{13}H_{28}$	mol = 6.67×10^{-14} x area	0.997
$C_{14}H_{30}$	mol = 6.15×10^{-14} x area	0.992
$C_{15}H_{32}$	mol = 6.25×10^{-14} x area	0.993

The calculation for the amount of each component in a standard-gas mixture can be calculated as follows:

$$\text{Amount of component}_i \text{ (mol)} = \frac{V_i \times T}{100 \times 22{,}400} \qquad \text{(A1)}$$

where V_i = % volume of component$_i$ (cm^3/cm^3)

T = volume of standard gases mixture (mL)

The calculation for the amount of each component in a standard liquids mixture that can be calculated as follows:

$$\text{Amount of component}_i \text{ (mol)} = \frac{V_i \times T \times D \times P \times 10^{-3}}{MW} \qquad \text{(A2)}$$

where V = % volume of component$_i$ (cm^3/cm^3)

T = volume of liquid mixture (μL)

D = density (g/cm^3)

P = purity (%)

MW = molecular weight (g/mol)

Appendix B

Conversion and Selectivity Results

Conversion and Selectivity Results

The calculation for the conversion of carbon monoxide to hydrocarbon products in Fischer-Tropsch synthesis (FTS) reaction are shown as follows:

Percent of CO conversion:

$$\text{CO conversion (\%)} = (CO_{in} - CO_{out})/CO_{in} \times 100$$

Percent of effluent composition for FTS products:

$$\text{Effluent composition of product}_i\ (\%) = \frac{\text{moles of product}_i \times 100}{\sum \text{moles of FTS products}}$$

Percent of hydrocarbon selectivity for hydrocarbon products:

$$\text{Selectivity of hydrocarbon}_i\ (\%) = \frac{\text{moles of hydrocarbon}_i \times 100}{(\sum \text{moles of hydrocarbon products}) \times n}$$

where CO_{in} is a mole number of inlet carbon monoxide

CO_{out} is a mole number of outlet carbon monoxide

n is a number of carbon atoms in hydrocarbon_i

Appendix Table B1 Calculation of CO conversion and selectivity of hydrocarbons over Co/SBA-15 catalyst

Description	Calculation
FTS reaction at T = 220 °C, P = 10 atm	
Inlet: CO amount (PV = nRT)	0.000006489 mol
Outlet: Peak areas of CO	21772
CO conversion	85.73 %
Peak areas of CH_4, C_2H_6, C_3H_8, C_4H_{10}	133,811, 7039, 5598, 19042
CH_4 amount (1.11×10^{-12} x area)	1.34×10^{-7} mol
C_2H_6 amount (5.22×10^{-13} x area)	3.52×10^{-9} mol
C_3H_8 amount (3.68×10^{-13} x area)	9.27×10^{-9} mol
C_4H_{10} amount (2.79×10^{-13} x area)	5.71×10^{-9} mol
C_6H_{14} amount	5.03×10^{-9} mol
$C_{10}H_{22}$ amount	4.71×10^{-9} mol
$C_{11}H_{24}$ amount	1.44×10^{-8} mol
$C_{12}H_{26}$ amount	8.88×10^{-9} mol
$C_{13}H_{28}$ amount	4.96×10^{-9} mol
$C_{14}H_{30}$ amount	4.67×10^{-10} mol
$C_{15}H_{32}$ amount	1.93×10^{-10} mol
Total hydrocarbons amount	2.17×10^{-7} mol
C_1 hydrocarbon selectivity	20.1 %
C_2 hydrocarbon selectivity	1.4 %
C_3 hydrocarbon selectivity	4.8 %
C_4 hydrocarbon selectivity	3.1 %

CIRRICULUM VITAE

NAME : Mr. Prasong Nakaew

BIRTH DATE : August 28, 1985

BIRTH PLACE : Chiang Rai, Thailand

EDUCATION :

YEAR	**INSTITUTE**	**DEGREE**
2008	Kasetsart Univ.	B.Eng. (Chemical)

SCHOLARSHIP : Teacher Assistant Scholarship from ADB Program of Department of Chemical Engineering, Kasetsart University 2008-2009